

RECEIVED: July 29, 2021

ACCEPTED: October 4, 2021

PUBLISHED: October 19, 2021

Measurement of the production cross section of prompt Ξ_c^0 baryons at midrapidity in pp collisions at $\sqrt{s} = 5.02 \text{ TeV}$



ALICE

The ALICE collaboration*E-mail:* ALICE-publications@cern.ch

ABSTRACT: The transverse momentum (p_T) differential cross section of the charm-strange baryon Ξ_c^0 is measured at midrapidity ($|y| < 0.5$) via its semileptonic decay into $e^+ \Xi^- \nu_e$ in pp collisions at $\sqrt{s} = 5.02 \text{ TeV}$ with the ALICE detector at the LHC. The ratio of the p_T -differential Ξ_c^0 -baryon and D^0 -meson production cross sections is also reported. The measurements are compared with simulations with different tunes of the PYTHIA 8 event generator, with predictions from a statistical hadronisation model (SHM) with a largely augmented set of charm-baryon states beyond the current lists of the Particle Data Group, and with models including hadronisation via quark coalescence. The p_T -integrated cross section of prompt Ξ_c^0 -baryon production at midrapidity is also reported, which is used to calculate the baryon-to-meson ratio $\Xi_c^0/D^0 = 0.20 \pm 0.04 \text{ (stat.)}^{+0.08}_{-0.07} \text{ (syst.)}$. These results provide an additional indication of a modification of the charm fragmentation from e^+e^- and e^-p collisions to pp collisions.

KEYWORDS: Heavy Ion Experiments**ARXIV EPRINT:** [2105.05616](https://arxiv.org/abs/2105.05616)

Contents

1	Introduction	1
2	Experimental apparatus and data sample	3
3	Data analysis	4
3.1	Reconstruction of e^\pm and Ξ^\pm candidates	4
3.2	Analysis of $e^\pm\Xi^\mp$ invariant mass distribution	5
3.3	Corrections and unfolding	6
3.4	Reconstruction efficiency and feed-down subtraction	8
3.5	Systematic uncertainties	10
4	Results	12
4.1	Comparison with model calculations	14
4.2	Extrapolation down to $p_T = 0$ of the Ξ_c^0 cross section and the Ξ_c^0/D^0 ratio	16
5	Summary and conclusions	16
The ALICE collaboration		23

1 Introduction

Measurements of the production of heavy-flavour hadrons (i.e. containing charm or beauty quarks) in high-energy hadronic collisions provide important tests of quantum chromodynamics (QCD) because perturbative techniques are applicable down to low transverse momentum (p_T) thanks to the large masses of charm and beauty quarks compared to the QCD scale parameter ($\Lambda_{\text{QCD}} \sim 200$ MeV). The production cross sections of heavy-flavour hadrons can be calculated using the factorisation approach [1] as a convolution of three factors: the parton distribution functions (PDFs) of the incoming protons, the hard-scattering cross section at partonic level, which can be calculated perturbatively in powers of the strong coupling constant α_s , and the fragmentation function, which parametrises the non-perturbative transition of a heavy quark into a given species of heavy-flavour hadron. The measurements of D- and B-meson production cross sections at midrapidity in proton-proton (pp) collisions at several centre-of-mass energies at the LHC [2–9] are described within uncertainties by perturbative calculations at next-to-leading order with next-to-leading-log resummation, such as the general-mass variable-flavour-number scheme (GM-VFNS [10–12]) and the fixed-order next-to-leading-log (FONLL [13, 14]) frameworks, over a wide range of p_T . Both calculations use fragmentation functions based on measurements in positron-electron (e^+e^-) collisions.

Measurements of the production cross sections of different charm-hadron species, comparing in particular baryon and meson production in various collision systems and centre-of-mass energies, provide insight into the properties of the fragmentation process. Measurements of Λ_c^+ -baryon production at midrapidity in pp collisions at $\sqrt{s} = 5.02, 7$, and 13 TeV were reported by the ALICE and CMS collaborations in refs. [15–19]. A clear decreasing trend of the Λ_c^+/D^0 ratio with increasing p_T is seen. The Λ_c^+/D^0 ratio is measured to be substantially larger than previous measurements at lower centre-of-mass energies in e^+e^- [20–22] and electron-proton (e^-p) collisions [23, 24], suggesting that the charm fragmentation is not universal among different collision systems. Similar indications were obtained from the measurements of $\Xi_c^{0,+}$ -baryon and $\Sigma_c^{0,++}$ -baryon production at midrapidity in pp collisions at $\sqrt{s} = 7$ and 13 TeV [19, 25, 26].

The charm-baryon production cross sections measured at the LHC are substantially larger than the predictions of GM-VFNS calculations and of the POWHEG next-to-leading-order (NLO) generator matched to PYTHIA 6 for the parton shower and the hadronisation stages [12, 17, 27]. Predictions from QCD-inspired event generators like PYTHIA 8 with Monash tune [28], DIPSY [29], and HERWIG 7 [30] also underestimate the baryon-to-meson ratios measured at midrapidity. On the other hand, PYTHIA 8 simulations with tunes including string formation beyond the leading-colour approximation [31] qualitatively describe the measured Λ_c^+/D^0 and $\Sigma_c^{0,+,++}/D^0$ ratios [17, 19], but underestimate the $\Xi_c^{0,+}/D^0$ ratio [25, 26]. Calculations with a statistical hadronisation model (SHM) [32] based on charm-hadron states listed by the Particle Data Group (PDG) [33] underestimate the measured baryon-to-meson ratios. The Λ_c^+/D^0 and $\Sigma_c^{0,+,++}/D^0$ ratios are qualitatively described by the SHM calculations if a larger set of yet-unobserved higher-mass charm-baryon states is considered under the guidance of the relativistic quark model (RQM) [34] and of lattice QCD [35]. However, the $\Xi_c^{0,+}/D^0$ ratios are still underestimated with the inclusion of the additional baryonic states [26]. An enhancement of the charmed baryon-to-meson ratio is expected also by models employing hadronisation of charm quarks via recombination in pp collisions [36, 37]. In the quark (re-)combination mechanism (QCM) model [36], the charm quark is combined with a co-moving light antiquark or with two co-moving quarks to form a charmed meson or baryon. The Catania model [37] implements charm-quark hadronisation via both coalescence, implemented via Wigner formalism [38], and fragmentation.

Finally, it should be noted that an increased yield of charmed baryons (Λ_c , Ξ_c , Ω_c) has significant consequences on the determination of the total charm cross section in pp collisions at the LHC [3, 4]. In the context of the heavy-ion programme at the LHC, the $c\bar{c}$ production cross section per nucleon-nucleon collision is a fundamental ingredient for the determination of the amount of charmonium production by (re)generation in a quark-gluon plasma (QGP), a mechanism that is supported by J/ψ measurements in nucleus-nucleus collisions at the LHC [39, 40]. A precise determination of the $c\bar{c}$ production cross section in pp collisions at midrapidity will offer a stronger constraint to models implementing J/ψ regeneration in the QGP [41–43]. In addition, measurements of open heavy-flavour baryon production in heavy-ion collisions provide a unique information on hadronisation mechanisms in the QGP. Models implementing charm-quark hadronisation via coalescence in addition to fragmentation [44–46] predict an enhanced baryon-to-meson ratio in heavy-ion collisions with respect to pp collisions.

In this article, we report the measurement of the p_T -differential production cross section of prompt Ξ_c^0 baryons in pp collisions at $\sqrt{s} = 5.02$ TeV and its ratio to the measured production cross section of prompt D^0 mesons (i.e. produced directly in the hadronisation of charm quarks and in the decays of directly produced excited charm states) [2, 9]. The Ξ_c^0 baryons and their antiparticles are reconstructed at midrapidity ($|y| < 0.5$) in the transverse momentum interval $2 < p_T < 8$ GeV/c via the semileptonic decay mode $\Xi_c^0 \rightarrow e^+ \Xi^- \nu_e$ and its charge conjugate. We have recently constrained the absolute branching ratio (BR) of this Ξ_c^0 decay in pp collision at $\sqrt{s} = 13$ TeV by measuring the Ξ_c^0 production via two different decay channels, $\Xi_c^0 \rightarrow e^+ \Xi^- \nu_e$ and $\Xi_c^0 \rightarrow \pi^+ \Xi^-$ [26]. This BR value is used in this analysis and it is also used to update the previously published measurement of inclusive Ξ_c^0 p_T -differential cross section in pp collisions at $\sqrt{s} = 7$ TeV [25].

The article is organised as follows. Section 2 describes the experimental setup, focusing on the detectors employed in the analysis and the data-taking conditions. The analysis details and the estimation of the systematic uncertainties are discussed in section 3. Section 4 presents the results, namely the p_T -differential production cross section of prompt Ξ_c^0 baryons and the Ξ_c^0/D^0 cross-section ratio, which are compared with different model calculations. The p_T -integrated production cross section of prompt Ξ_c^0 baryons, and the corresponding Ξ_c^0/D^0 ratio, extrapolated down to $p_T = 0$, are also reported and compared with model calculations. Finally, conclusions are drawn in section 5.

2 Experimental apparatus and data sample

The ALICE apparatus, described in detail in refs. [47, 48], consists of a central barrel covering the pseudorapidity region $|\eta| < 0.9$ placed inside a solenoidal magnet that provides a $B = 0.5$ T field parallel to the beam direction, a muon spectrometer at forward pseudorapidity ($-4 < \eta < -2.5$), and a set of detectors at forward/backward rapidity for triggering and event selection. The detectors used for reconstruction and identification of the Ξ_c^0 decay products are the Inner Tracking System (ITS) [49], the Time Projection Chamber (TPC) [50], and the Time-Of-Flight detector (TOF) [51]. The ITS consists of six cylindrical layers of silicon detectors. The two innermost layers, equipped with Silicon Pixel Detectors (SPD), provide a space-point position resolution of $12\ \mu\text{m}$ and $100\ \mu\text{m}$ in the $r\varphi$ and the beam direction, respectively. The third and fourth layers consist of Silicon Drift Detectors (SDD), while the two outermost layers are equipped with Silicon Strip Detectors (SSD).

The TPC is the main tracking detector in the central barrel. With up to 159 space points to reconstruct the charged-particle trajectory, it provides charged-particle momentum measurement together with excellent two-track separation and particle identification via dE/dx determination with a resolution better than 5% [50].

The TOF detector provides the measurement of the flight time of charged particles from the interaction point to the detector radius of 3.8 m, with an overall resolution of about 80 ps. The collision time is obtained using either the information from the T0 detector [52], or the TOF detector, or a combination of the two. The T0 detector consists of two arrays of Čerenkov counters, located on both sides of the interaction point, covering the pseudorapidity intervals $-3.28 < \eta < -2.97$ and $4.61 < \eta < 4.92$.

The V0 detector [53], composed of two arrays of 32 scintillators each, covering the pseudorapidity intervals $-3.7 < \eta < -1.7$ and $2.8 < \eta < 5.1$, provides the minimum bias (MB) trigger used to collect the data sample. In addition, the timing information of the two V0 arrays and the correlation between the number of hits and track segments in the SPD were used for an offline event selection, in order to remove background due to interactions between one of the beams and the residual gas present in the beam vacuum tube.

In order to maintain a uniform acceptance in pseudorapidity, collision vertices were required to be within ± 10 cm from the centre of the detector along the beam line direction. The pile-up events (less than 1%) were rejected by detecting multiple primary vertices using track segments defined with the SPD layers. After the aforementioned selections, the data sample used for the analysis consists of about 990 million MB events, corresponding to an integrated luminosity of $\mathcal{L}_{\text{int}} = (19.3 \pm 0.4) \text{ nb}^{-1}$ [54], collected during the 2017 pp run at $\sqrt{s} = 5.02 \text{ TeV}$.

3 Data analysis

The analysis is performed using similar techniques to those reported in ref. [25]. The Ξ_c^0 baryons are reconstructed via the semileptonic decay mode $\Xi_c^0 \rightarrow e^+ \Xi^- \nu_e$, and its charge conjugate. The Ξ_c^0 candidates are defined from $e^+ \Xi^-$ pairs formed by combining positrons and Ξ^- baryons. The Ξ_c^0 raw yield is obtained by counting the $e^+ \Xi^-$ pairs in $p_T^{e\Xi}$ intervals, where $p_T^{e\Xi}$ is the transverse momentum of the $e^+ \Xi^-$ pair, after subtracting the combinatorial background, as described in section 3.2. The $p_T^{e\Xi}$ distribution of $e^+ \Xi^-$ pairs is corrected for the missing momentum of the neutrino using unfolding techniques, in order to obtain the Ξ_c^0 raw yield in intervals of $\Xi_c^0 p_T$, as described in section 3.3. The contribution of Ξ_c^0 baryons originating from beauty-hadron decays is subtracted from the measured yield by using perturbative quantum chromodynamics (pQCD) calculations of the beauty-quark cross section together with the fragmentation fractions of beauty quarks into hadrons measured by LHCb [55], and the acceptance and efficiency values estimated from simulations as described in section 3.4. Charge conjugate modes are implied everywhere, unless otherwise stated. The final results are obtained as the average of particles and antiparticles.

3.1 Reconstruction of e^\pm and Ξ^\pm candidates

Candidate electron and positron tracks satisfying $|\eta| < 0.8$ and $p_T > 0.5 \text{ GeV}/c$ are required to have a number of crossed TPC pad rows larger than 80, a χ^2 normalised to the number of associated TPC clusters smaller than 4, and at least 3 hits in the ITS. These selection criteria suppress the contribution from short tracks, which are unlikely to originate from the primary vertex. In order to reject electrons from photon conversions occurring in the detector material outside the innermost SPD layer, the electron candidate tracks are required to have associated hits in the two SPD layers of the ITS [56, 57]. In addition, at least 50 TPC clusters are required for the calculation of the dE/dx signal. Electrons are identified using the dE/dx and the time-of-flight measurements in the TPC and TOF detectors. The selection is applied on the $n_{\sigma,e}^{\text{TPC}}$ and $n_{\sigma,e}^{\text{TOF}}$ variables defined as the difference between the measured dE/dx or time-of-flight values and the ones expected

for electrons, divided by the corresponding detector resolution. In the left panel of figure 1, the $n_{\sigma,e}^{\text{TPC}}$ distribution as a function of the candidate electron p_T is shown for tracks with a time-of-flight compatible with the value expected for an electron within $|n_{\sigma,e}^{\text{TOF}}| < 3$. The following criterion is applied on the TPC dE/dx signal to select electron candidates:

$$-3.9 + 1.2p_T - 0.094p_T^2 < |n_{\sigma,e}^{\text{TPC}}(p_T)| < 3$$

(with p_T in units of GeV/c), which is represented by the red lines in the left panel of figure 1. The p_T -dependent lower limit on $|n_{\sigma,e}^{\text{TPC}}|$ is optimised to reject hadrons. An electron purity of 98% is achieved over the whole p_T range.

Further rejection of background electrons originating from Dalitz decays of neutral mesons and photon conversions in the detector material (“photonic” electrons) is obtained using a technique based on the invariant mass of e^+e^- pairs [40, 58]. The electron (positron) candidates are paired with opposite-sign tracks from the same event passing loose identification criteria ($|n_{\sigma,e}^{\text{TPC}}| < 5$ without any TOF requirement) and are rejected if they form at least one e^+e^- pair with an invariant mass smaller than $50 \text{ MeV}/c^2$. Loose electron identification criteria are used in order to have a high efficiency of finding the partners [59]. With this selection the fraction of signal lost due to mistagging is less than 2%, as discussed in section 3.3.

The Ξ^- baryons are reconstructed from the decay chain $\Xi^- \rightarrow \Lambda\pi^-$ ($\text{BR} = 99.887 \pm 0.035\%$), followed by $\Lambda \rightarrow p\pi^-$ ($\text{BR} = 63.9 \pm 0.5\%$) [33]. Tracks used to define Ξ^- candidates are required to have a number of crossed TPC pad rows larger than 70 and a dE/dx signal in the TPC consistent with the expected value for protons (pions) within 4σ . The Ξ^- and Λ baryons have long lifetimes ($c\tau$ of about 4.91 cm and 7.89 cm, respectively [33]), and thus they can be selected exploiting their characteristic decay topologies [60]. Pions originating directly from Ξ^- decays are selected by requiring a minimum distance of closest approach (d_0) of their tracks to the primary vertex, $d_0 > 0.05$ cm, while protons and pions originating from Λ decays are required to have $d_0 > 0.07$ cm. The d_0 of the Λ trajectory to the primary vertex is required to be larger than 0.05 cm, while the cosine of the Λ pointing angle, which is the angle between the reconstructed Λ momentum and the line connecting the Λ and Ξ^- decay vertices, is required to be larger than 0.98. The cosine of the pointing angle of the reconstructed Ξ^- momentum to the primary vertex is required to be larger than 0.983. The radial distances of the Ξ^- and Λ decay vertices from the beam line are required to be larger than 0.4 and 2.7 cm, respectively. These selection criteria are tuned to reduce the background and enhance the purity of the signal. In the right panel of figure 1 the Ξ^- peak in the $\pi^-\Lambda$ invariant mass distribution integrated for $p_T^{\Xi^-} > 0$ is shown. Only Ξ^- candidates with invariant masses within $8 \text{ MeV}/c^2$ from the world average Ξ^- mass ($1321.71 \pm 0.07 \text{ MeV}/c^2$ [33]), indicated by an arrow in the right panel of figure 1, are kept for further analysis.

3.2 Analysis of $e^\pm\Xi^\mp$ invariant mass distribution

The Ξ_c^0 candidates are defined from $e^+\Xi^-$ pairs. Only pairs with an opening angle smaller than 90 degrees are used for the analysis. Due to the undetected neutrino, the invariant mass distribution of $e^+\Xi^-$ pairs does not show a peak at the Ξ_c^0 mass. Following the same approach adopted and described in ref. [25], the background contributions are estimated

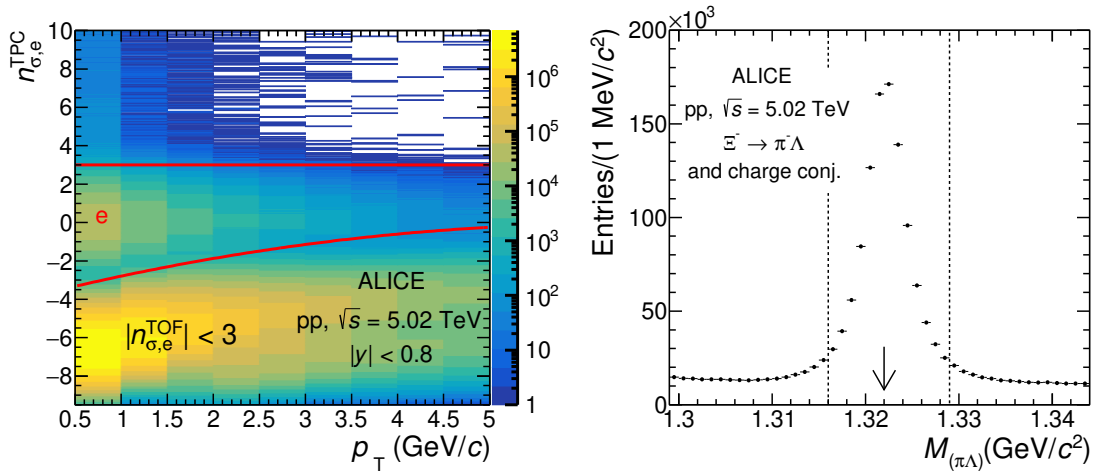


Figure 1. Left panel: $n_{\sigma,e}^{\text{TPC}}$ distribution as a function of the electron p_T after applying the particle identification criteria on the TOF signal (see text for details). Right panel: invariant mass distribution of $\Xi^- \rightarrow \pi^-\Lambda$ (and charge conjugate) candidates integrated over $p_T^{\Xi^-}$. The arrow indicates the world average Ξ^- mass [33] and the dashed lines define the interval in which the Ξ^- candidates are selected for the Ξ_c^0 reconstruction (see text for details).

exploiting the fact that Ξ_c^0 baryons and their antiparticles decay only into $e\Xi$ pairs with opposite charge sign ($e^+\Xi^-$ and $e^-\Xi^+$), denoted as right-sign (RS), and not into same-sign pairs ($e^-\Xi^-$ and $e^+\Xi^+$), denoted as wrong-sign (WS), while combinatorial background candidates contribute equally to both RS and WS pairs. The Ξ_c^0 raw yield is obtained from the invariant mass distribution of RS pairs after subtracting the WS contribution. Other contributions to $e\Xi$ pairs, such as those from $\Xi_b^{0,-}$ semileptonic decays to WS pairs, which do not give rise to RS pairs, are corrected for after the subtraction, as described in section 3.3. In the left panel of figure 2 the uncorrected invariant mass distributions of WS and RS pairs in the interval $2 < p_T^{e\Xi} < 8 \text{ GeV}/c$ are shown for illustration. In the right panel of figure 2 the invariant mass distribution of Ξ_c^0 candidates obtained after subtracting the WS pair yield from the RS yield is shown. Only $e^+\Xi^-$ pairs satisfying $m_{e\Xi} < 2.5 \text{ GeV}/c^2$ are considered.

3.3 Corrections and unfolding

The raw yield obtained by counting the $e^+\Xi^-$ candidates in bins of $p_T^{e\Xi}$ after the subtraction of the WS pairs needs to be corrected for the signal loss due to mistagging of photonic electrons, and for the $\Xi_b^{0,-}$ contribution in the WS pairs. Finally, the $p_T^{e\Xi}$ -differential spectrum is corrected for the missing neutrino momentum to obtain the Ξ_c^0 raw yield in intervals of $\Xi_c^0 p_T$.

The probability of wrongly tagging an electron as photonic is estimated by applying the tagging algorithm, described in section 3.1, to e^+e^+ and e^-e^- pairs. The resulting correction is smaller than 2%, with a mild dependence on the p_T of the $e^+\Xi^-$ pair, as it was also observed in refs. [25, 26].

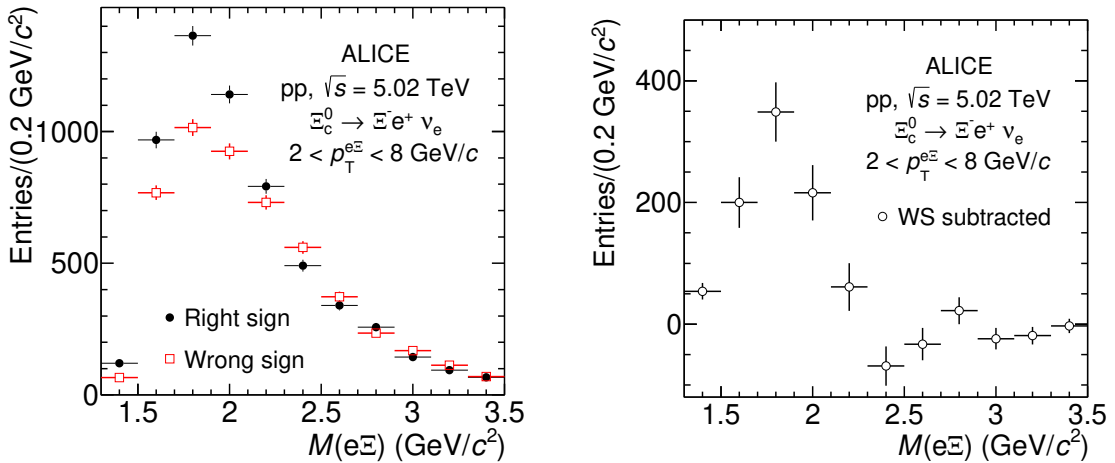


Figure 2. Left panel: invariant mass distributions of right-sign and wrong-sign $e\Xi$ pairs with $2 < p_T < 8 \text{ GeV}/c$. Right panel: invariant mass distribution of Ξ_c^0 candidates obtained by subtracting the wrong-sign pair yield from the right-sign pair yield.

Decays of $\Xi_b^{0,-}$ to electrons, $\Xi_b^{0,-} \rightarrow H_c e^- X$ (where H_c is any charmed baryon), followed by H_c decays to Ξ^- , $H_c \rightarrow \Xi^- X$, contribute to the WS invariant mass distribution and not to the RS one, giving rise to a background over-subtraction. In order to estimate this contribution, assumptions must be made for the branching ratio of $\Xi_b^{0,-}$ into $e^- \Xi^- \bar{\nu}_e X$ and for the $\Xi_b^{0,-}$ production cross sections, which are not measured. First, the shape of the transverse momentum distribution of $\Xi_b^{0,-}$ baryons is assumed to be the same as that of Λ_b^0 baryons. The CMS collaboration reported a measurement of the p_T -differential Λ_b^0 production cross section multiplied by the $\text{BR}(\Lambda_b^0 \rightarrow J/\psi \Lambda)$ in pp collisions at $\sqrt{s} = 7 \text{ TeV}$ [61]. To scale the Λ_b^0 measurement at the centre-of-mass energy of 5.02 TeV, the ratio of the beauty-hadron cross sections at $\sqrt{s} = 7 \text{ TeV}$ and 5.02 TeV obtained with FONLL pQCD calculations is used [13, 14]. The second assumption is that the fraction of beauty quarks that hadronise into Λ_b^0 and $\Xi_b^{0,-}$ are the same as those in $e^+ e^-$ collisions. The yield of $\Xi_b^{0,-} \rightarrow e^- \Xi^- \bar{\nu}_e X$ is therefore computed using i) the \sqrt{s} -scaled Λ_b^0 cross section, ii) the values of $f(b \rightarrow \Xi_b^{0,-}) \times \text{BR}(\Xi_b^{0,-} \rightarrow e^- \Xi^- \bar{\nu}_e X)$ [33] and $f(b \rightarrow \Lambda_b^0) \times \text{BR}(\Lambda_b^0 \rightarrow J/\psi \Lambda)$ [62] measured in $e^+ e^-$ collisions, and iii) the $\Xi_b^{0,-} \rightarrow e^- \Xi^- \bar{\nu}_e X$ acceptance \times efficiency ($\text{Acc} \times \varepsilon$) from the simulations described below. The contribution to the WS pair yield from $\Xi_b^{0,-}$ baryon decays is estimated to be about 2%.

The correction for the missing momentum of the neutrino is performed by using an unfolding technique with a response matrix which represents the correlation between the p_T of the Ξ_c^0 baryon and that of the reconstructed $e^+ \Xi^-$ pair. The response matrix is determined through a simulation with the PYTHIA 8.243 event generator [63] and the GEANT 3 transport code [64], including a realistic description of the detector conditions and alignment during the data taking period. The response matrix needs to be determined using a realistic Ξ_c^0 -baryon p_T distribution which is not known a priori. Therefore, a two-step iterative procedure is adopted. In the first step, the response matrix is obtained with

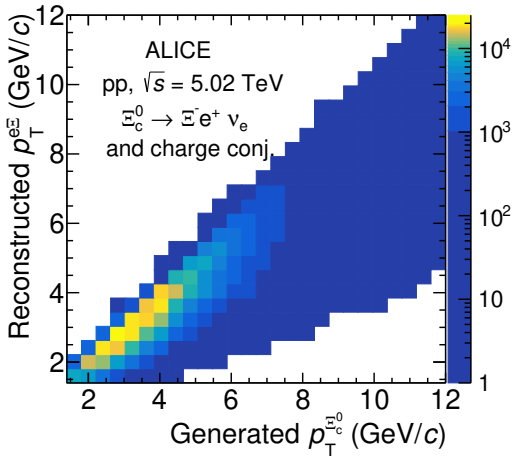


Figure 3. Correlation matrix between the generated Ξ_c^0 -baryon p_T and the reconstructed $e^+\Xi^-$ pair p_T , obtained from the simulation based on PYTHIA 8 described in the text.

the p_T distribution generated with PYTHIA 8. This matrix is used to calculate a first estimate of the Ξ_c^0 p_T -differential spectrum from the measured p_T distribution of $e^+\Xi^-$ pairs. The Ξ_c^0 p_T distribution from this first iteration is used to reweight the response matrix, which is then used for the second iteration. The response matrix obtained from this procedure is shown in figure 3. The Bayesian unfolding technique [65] implemented in the RooUnfold package [66] is used. In this analysis the Bayesian procedure required three iterations to converge. The response matrix used in the unfolding procedure is defined in the transverse momentum interval $1.4 < p_T < 12 \text{ GeV}/c$, which is wider than the p_T interval used for the cross section measurement, to avoid edge effects at the lowest and highest p_T intervals of the measurement.

3.4 Reconstruction efficiency and feed-down subtraction

The p_T -differential cross section of prompt Ξ_c^0 -baryon production is obtained as

$$\frac{d^2\sigma^{\Xi_c^0}}{dp_T dy} = \frac{1}{BR} \times \frac{1}{2\Delta y \Delta p_T} \times \frac{f_{\text{prompt}} \times N_{\text{raw}}^{\Xi_c^0 + \bar{\Xi}_c^0}}{(Acc \times \varepsilon)_{\text{prompt}}} \times \frac{1}{\mathcal{L}_{\text{int}}}, \quad (3.1)$$

where $N_{\text{raw}}^{\Xi_c^0 + \bar{\Xi}_c^0}$ is the raw yield after the unfolding correction in a given p_T interval with width Δp_T , f_{prompt} is the fraction of prompt Ξ_c^0 in the raw yield of Ξ_c^0 , BR is the branching ratio for the considered decay mode, and \mathcal{L}_{int} is the integrated luminosity. The $(Acc \times \varepsilon)_{\text{prompt}}$ factor is the product of detector acceptance and efficiency for prompt Ξ_c^0 baryons, where ε accounts for the reconstruction and selection of the Ξ_c^0 decay-product tracks and the Ξ_c^0 -candidate selection. The factor Δy represents the width of the rapidity interval in which the generated Ξ_c^0 are considered and it is applied to obtain the cross section in one unit of rapidity. The factor 1/2 takes into account that $N_{\text{raw}}^{\Xi_c^0}$ includes both particles and antiparticles, while the cross section is given for particles only. The BR of the considered semileptonic decay channel is calculated from the ratio $BR(\Xi_c^0 \rightarrow \Xi^- e^+ \nu_e)/BR(\Xi_c^0 \rightarrow$

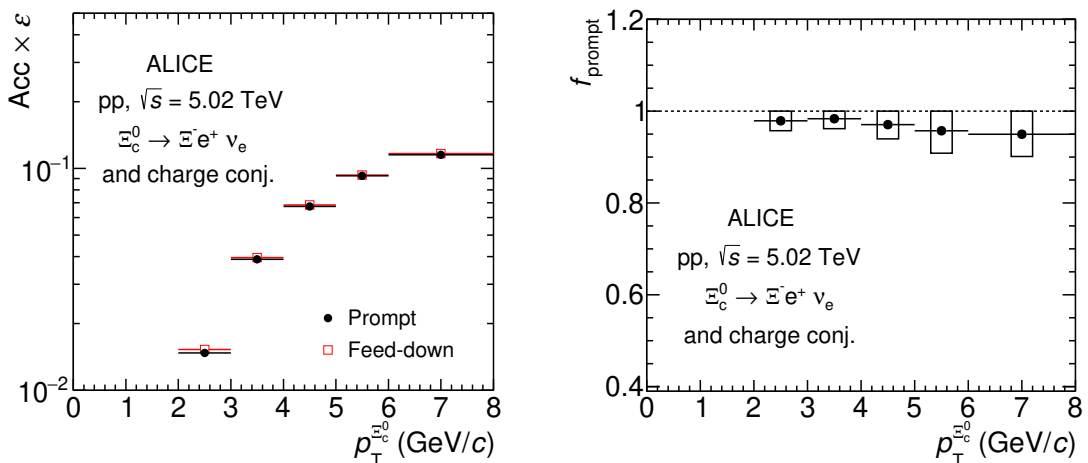


Figure 4. Left panel: product of acceptance and efficiency for prompt and feed-down Ξ_c^0 baryons in pp collisions at $\sqrt{s} = 5.02$ TeV as a function of p_T . Right panel: fraction of prompt Ξ_c^0 baryons in the raw yield (f_{prompt}) as a function of p_T . The systematic uncertainties of f_{prompt} are shown as boxes.

$\Xi^- \pi^+ = 1.36 \pm 0.14 \text{ (stat.)} \pm 0.19 \text{ (syst.)}$, measured by ALICE in pp collisions at $\sqrt{s} = 13$ TeV [26], which is multiplied by the hadronic decay branching ratio $\text{BR}(\Xi_c^0 \rightarrow \Xi^- \pi^+)$ reported in the PDG [33] to get $\text{BR}(\Xi_c^0 \rightarrow \Xi^- e^+ \nu_e) = (1.94 \pm 0.55)\%$.

The $(\text{Acc} \times \epsilon)$ factor is obtained from the same simulations used to determine the response matrix in which the detector and data taking conditions are reproduced. The $(\text{Acc} \times \epsilon)$ is computed separately for prompt and feed-down (produced in beauty-hadron decays) Ξ_c^0 baryons and is reported in the left panel of figure 4. The efficiencies of prompt and feed-down baryons are consistent with each other within uncertainties because the applied selection criteria are not sensitive to the displacement by a few hundred micrometers of the prompt and feed-down Ξ_c^0 decay vertices from the collision point. In order to compute the efficiency with a realistic momentum distribution of Ξ_c^0 baryons, the p_T shape of the Ξ_c^0 baryons from the PYTHIA 8 simulation is reweighted to match the measured one via a two-step iterative procedure similar to the one used for the response matrix.

The factor f_{prompt} is calculated as

$$f_{\text{prompt}} = 1 - \frac{N_{\text{raw}}^{\Xi_c^0 \text{ feed-down}}}{N_{\text{raw}}^{\Xi_c^0 + \bar{\Xi}_c^0}/2} = 1 - \frac{(\text{Acc} \times \epsilon)_{\text{feed-down}} \cdot \Delta y \cdot \Delta p_T \cdot \text{BR} \cdot \mathcal{L}_{\text{int}}}{N_{\text{raw}}^{\Xi_c^0 + \bar{\Xi}_c^0}/2} \times \left(\frac{d^2\sigma}{dp_T dy} \right)_{\Xi_c^0 \text{ feed-down}}, \quad (3.2)$$

where $N_{\text{raw}}^{\Xi_c^0 + \bar{\Xi}_c^0}/2$ is the raw yield divided by a factor of two to account for particles and antiparticles, $(\text{Acc} \times \epsilon)_{\text{feed-down}}$ is the product of detector acceptance and efficiency for feed-down Ξ_c^0 baryons and $\left(\frac{d^2\sigma}{dp_T dy} \right)_{\Xi_c^0 \text{ feed-down}}$ is the p_T -differential cross section of feed-down Ξ_c^0 baryon production. The production cross section of Ξ_c^0 from beauty-baryon decays is not known, hence a strategy based on the estimation made in ref. [17] for the cross section of feed-down Λ_c^+ is adopted. The production cross section of Λ_c^+ from Λ_b^0 -baryon decays is calculated using the b-quark p_T -differential cross section from FONLL calculations, multi-

plied by the fraction of beauty quarks that fragment into Λ_b^0 . The latter is derived from the LHCb measurement of beauty fragmentation fractions in pp collisions at $\sqrt{s} = 13$ TeV [55], taking into account its p_T dependence. The $\Lambda_b^0 \rightarrow \Lambda_c^+ + X$ decay kinematics is modeled using PYTHIA 8.243 simulations [63]. The cross section of Λ_c^+ from Λ_b^0 -baryon decays is scaled by the fraction of Ξ_b^- decaying in a final state with a Ξ_c^0 over the fraction of Λ_b^0 decaying to Λ_c^+ , which are taken to be 50% and 82%, respectively, from the PYTHIA 8.243 generator [63]. The cross section of Ξ_c^0 from beauty feed-down is then calculated from the cross section of Λ_c^+ originating from Λ_b^0 decays, which is scaled by the ratio of the measured p_T -differential yields of inclusive Ξ_c^0 and prompt Λ_c^+ baryons. This procedure relies on the assumptions that the p_T shape of the cross sections of feed-down Λ_c^+ and Ξ_c^0 is the same and that the ratio Ξ_c^0/Λ_c^+ is the same for inclusive and feed-down baryons, along with the consideration that the inclusive Λ_c^+ -baryon yield is dominated by the prompt production, based on the f_{prompt} values close to unity reported in ref. [18]. The value of f_{prompt} as a function of p_T is shown in the right panel of figure 4.

3.5 Systematic uncertainties

The systematic uncertainty on the Ξ_c^0 production cross section has different contributions, which are summarised in table 1 for three representative p_T intervals, namely $2 < p_T < 3$ GeV/ c , $4 < p_T < 5$ GeV/ c , and $6 < p_T < 8$ GeV/ c , and discussed in the following. The overall systematic uncertainty is calculated summing in quadrature the different contributions, which are assumed to be uncorrelated among each other.

The systematic uncertainty on the tracking efficiency is estimated by comparing the probability of prolonging a track from the TPC to the ITS (“matching efficiency”) in data and simulation, and by varying the track-selection criteria in the analysis. The uncertainty on the matching efficiency affects only the electron track, and not the tracks of the Ξ^- decay particles, for which the prolongation to ITS is not required. It is defined as the relative difference in the ITS-TPC matching efficiency between simulation and data. The uncertainty, which slightly depends on the track p_T , is propagated from the electron track to the Ξ_c^0 taking into account the decay kinematics and is 2% independent of $\Xi_c^0 p_T$. The second contribution to the track reconstruction uncertainty is estimated by repeating the analysis varying the TPC track selection criteria separately for the electron track and for the Ξ^- daughter tracks. The uncertainty is obtained from the root mean square (RMS) of the Ξ_c^0 cross section values obtained with the different track selection criteria and is 2% for the electron track and 4% for the Ξ^- daughters independent of $\Xi_c^0 p_T$.

Systematic uncertainties can arise from discrepancies in the particle-identification efficiency between simulation and data. The analysis is repeated by varying the selection criteria applied to identify the electron candidate tracks. The systematic uncertainty ranges from 4% to 7% depending on the $\Xi_c^0 p_T$.

The systematic uncertainty of the efficiency correction for the Ξ^- topological selection is 6% and it is estimated from the RMS of the distribution of the Ξ_c^0 corrected yields, when the Ξ^- topological selection criteria are varied relative to the default measurement.

The uncertainty of the $e^+\Xi^-$ -pair selection efficiency is estimated by varying the selection criteria of the opening angle and the invariant mass of the pair. A 3% uncertainty is assigned, independent of $\Xi_c^0 p_T$.

p_T (GeV/c)	2–3	4–5	6–8
ITS-TPC matching	2%	2%	2%
Electron track selection	2%	2%	2%
Ξ^\pm -daughter track selection	4%	4%	4%
Electron identification	4%	7%	5%
Ξ^\pm topological selection	6%	6%	6%
e Ξ -pair selection	3%	3%	3%
Bayesian-unfolding iterations	5%	9%	2%
Unfolding method	5%	6%	4%
Response-matrix p_T range and binning	6%	—	—
Ξ_b oversubtraction	1%	1%	1%
Generated p_T shape	2%	2%	2%
Sensitivity to rapidity interval	4%	4%	4%
Feed-down subtraction	$^{+2\%}_{-2\%}$	$^{+3\%}_{-3\%}$	$^{+5\%}_{-5\%}$
Total systematic uncertainty	$^{+14\%}_{-14\%}$	$^{+16\%}_{-16\%}$	$^{+13\%}_{-13\%}$
Branching ratio	28.4%		
Luminosity	2.1%		

Table 1. Contributions to the systematic uncertainty of the Ξ_c^0 cross section for the p_T intervals $2 < p_T < 3 \text{ GeV}/c$, $4 < p_T < 5 \text{ GeV}/c$, and $6 < p_T < 8 \text{ GeV}/c$.

The systematic uncertainty of the correction for the missing neutrino momentum is studied testing the stability of the results when varying the unfolding procedure. As a first test, the number of iterations in the Bayesian unfolding procedure is varied. The contribution ranges from 5% (9%) at low (intermediate) p_T to 2% in the highest p_T interval of the measurement. The second contribution arises from the variation of the unfolding method. The Singular Value Decomposition (SVD) method [67] is used and a p_T -dependent systematic uncertainty between 4% and 7% is assigned based on the difference with respect to the Bayesian method. The last contribution is related to the p_T range and the binning of the response matrix used in the unfolding. Systematic uncertainties of 6% and 4% are assigned in the intervals $2 < p_T < 3 \text{ GeV}/c$ and $3 < p_T < 4 \text{ GeV}/c$, respectively. At higher p_T , this contribution is negligible. For these three contributions, the systematic uncertainty is defined as the RMS of the yield values obtained after the unfolding.

The systematic uncertainty due to the subtraction of the $\Xi_b^{0,-}$ contribution to the WS pairs is estimated by varying the $\Xi_b^{0,-}$ yield and momentum distribution based on the uncertainties of the Λ_b^0 p_T -differential cross section in pp collisions [61]. The assigned systematic uncertainty is 1%, independent of Ξ_c^0 p_T .

The systematic uncertainty due to the uncertainty of the generated Ξ_c^0 p_T shape used in the determination of the efficiency is estimated by using the shape from the PYTHIA 8

generator instead of the one from the iterative procedure and is found to be 2%, independent of p_T . An additional source of uncertainty originates from possible differences between the Ξ_c^0 -rapidity distributions in data and in the simulation, which affect the measured cross section because the $(\text{Acc} \times \varepsilon)$ depends on the Ξ_c^0 rapidity. The systematic uncertainty is estimated to be 4% by comparing the cross section values obtained using the values of $(\text{Acc} \times \varepsilon)$ and Δy obtained considering the generated Ξ_c^0 baryons in different rapidity intervals (from $|y| < 0.5$ to $|y| < 0.8$).

The systematic uncertainty due to the subtraction of the feed-down from beauty-hadron decays is estimated by considering the uncertainty on the FONLL predictions and by varying the assumption on the ratio Ξ_c^0/Λ_c^+ in the f_{prompt} calculation. The FONLL uncertainty is calculated by varying the b-quark mass and the factorisation and renormalisation scales as prescribed in ref. [14]. The ratio of inclusive Ξ_c^0 over prompt Λ_c^+ yield, used to multiply the feed-down Ξ_c^0 cross section, is scaled up by a factor of 2 to account for possible differences between the Ξ_c^0/Λ_c^+ and $\Xi_b^{0,-}/\Lambda_b^0$ ratios, and scaled down in order to cover the $\Xi_b^{0,-}/\Lambda_b^0$ value of about 0.12 measured at forward rapidity by the LHCb collaboration [68]. The uncertainty ranges between 2% and 5% depending on the p_T interval. An alternative method for the estimation of the f_{prompt} factor, which consists in the usage of the prompt and feed-down Ξ_c^0 yields generated with PYTHIA 8 colour reconnection (CR) Mode 2 [31], was tested and the obtained results are compatible with the method described above and therefore no systematic uncertainty from this additional method is considered.

All the different sources of systematic uncertainty are considered correlated among the different p_T intervals except the systematic uncertainties due to the unfolding and the pair selection. The p_T -differential cross section has an additional global normalisation uncertainty due to the uncertainties of the integrated luminosity [54] and the branching ratio. These contributions are not summed in quadrature with the other sources of uncertainty in figure 5 and 6.

4 Results

The p_T -differential cross section of prompt Ξ_c^0 -baryon production in pp collisions at $\sqrt{s} = 5.02$ TeV, measured in the rapidity interval $|y| < 0.5$ and p_T range $2 < p_T < 8$ GeV/ c , is shown in the left panel of figure 5. It is compared with the previously published measurements of inclusive Ξ_c^0 -baryon production in pp collisions at $\sqrt{s} = 7$ TeV [25], updated with the BR value from ref. [26], and of prompt Ξ_c^0 -baryon production at $\sqrt{s} = 13$ TeV [26], which is measured as the average of two decay channels ($\Xi_c^0 \rightarrow \Xi^- e^+ \nu_e$ and $\Xi_c^0 \rightarrow \Xi^- \pi^+$). The prompt fraction in the Ξ_c^0 -baryon yield is close to unity (see right panel of figure 4), hence the comparison of the inclusive Ξ_c^0 cross section measured at $\sqrt{s} = 7$ TeV with the prompt ones at $\sqrt{s} = 5$ and 13 TeV provides a meaningful insight into the \sqrt{s} dependence of the production cross section. The vertical bars and empty boxes represent the statistical and systematic uncertainties. The systematic uncertainties of the BR are shown as shaded boxes. The uncertainty of the integrated luminosity is not included in the boxes. The data points are positioned at the centre of the p_T intervals. As expected, a smaller Ξ_c^0 production cross section is measured at lower collision energies. The difference between the

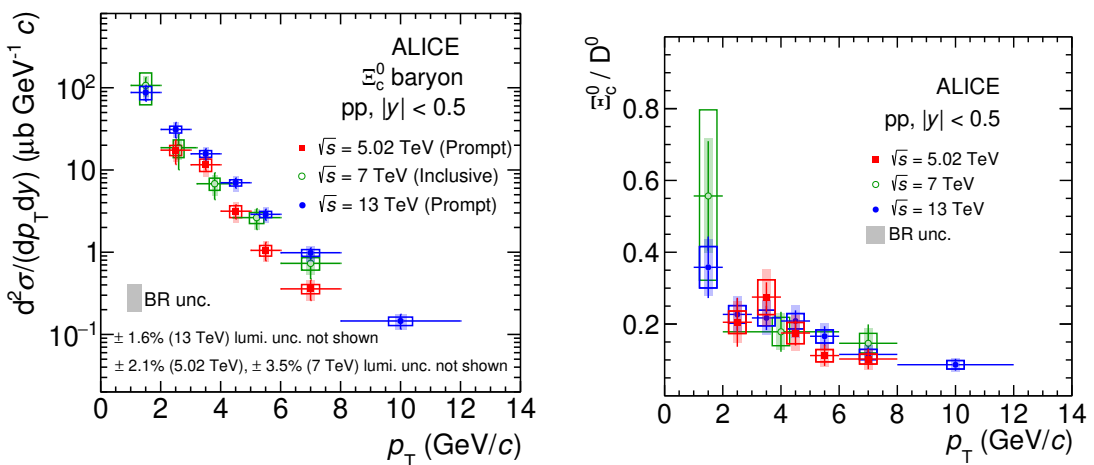


Figure 5. Left panel: p_T -differential production cross sections of prompt Ξ_c^0 baryons in pp collisions at $\sqrt{s} = 5.02 \text{ TeV}$ and 13 TeV [26] and of inclusive Ξ_c^0 baryons in pp collisions at $\sqrt{s} = 7 \text{ TeV}$ [25] with updated decay BR as discussed in the text. The uncertainty of the BR of the cross sections of prompt Ξ_c^0 baryons in pp collisions at $\sqrt{s} = 13 \text{ TeV}$ is lower because it consists in the combination of two different decay channels ($\Xi_c^0 \rightarrow e^+ \Xi^- \nu_e$ and $\Xi_c^0 \rightarrow \pi^+ \Xi^-$) [26]. Right panel: Ξ_c^0/D^0 ratio measured in pp collisions at $\sqrt{s} = 5.02 \text{ TeV}$, compared with the measurements at $\sqrt{s} = 7 \text{ TeV}$ [25] and $\sqrt{s} = 13 \text{ TeV}$ [26]. The uncertainty of the BR of D^0 and Ξ_c^0 are shown as shaded boxes.

cross sections at different \sqrt{s} values increases with increasing p_T , indicating a hardening of the p_T -differential spectrum with increasing collision energy. This behaviour is consistent with that observed for the D-meson and Λ_c^+ -baryon cross sections at $\sqrt{s} = 5.02$, 7 and 13 TeV [2, 3, 16, 18, 19], and with the expectations from pQCD calculations [13, 14]. The visible cross section is computed by integrating the p_T -differential cross section in the p_T interval of the measurement.

$$\frac{d\sigma_{\text{pp}, 5.02 \text{ TeV}}^{\Xi_c^0}}{dy} \Big|_{|y| < 0.5}^{(2 < p_T < 8 \text{ GeV}/c)} = 33.9 \pm 6.0 \text{ (stat.)} \pm 10.6 \text{ (syst.)} \pm 0.7 \text{ (lumi.) } \mu\text{b.} \quad (4.1)$$

The BR uncertainty is included in the systematic uncertainty.

In the right panel of figure 5 the Ξ_c^0/D^0 cross section ratio measured in pp collisions at $\sqrt{s} = 5.02 \text{ TeV}$ as a function of p_T is shown and compared with the same baryon-to-meson ratio measured at $\sqrt{s} = 7$ [25] and 13 TeV [26]. The prompt D^0 cross section is reported in ref. [9] in finer p_T intervals than those used in the prompt Ξ_c^0 analysis and is thus rebinned to match the p_T intervals of the Ξ_c^0 measurement. When merging the D^0 cross section in different p_T intervals, the systematic uncertainties are propagated considering the yield extraction uncertainty as fully uncorrelated and all the other sources as fully correlated among the p_T intervals. The systematic uncertainty on the Ξ_c^0/D^0 ratio is calculated assuming all the uncertainties of the Ξ_c^0 and D^0 cross sections as uncorrelated, except for the tracking and feed-down systematic uncertainties, which partially cancel in the ratio. The uncertainty of the luminosity fully cancels in the baryon-to-meson ratio. The Ξ_c^0/D^0 ratios at the three centre-of-mass energies are consistent with each other within

uncertainties. At low p_T , the ratio is about 0.2 and it decreases with increasing p_T , reaching a value of about 0.1 for $p_T > 6 \text{ GeV}/c$. The Ξ_c^0/D^0 ratio in pp collisions at $\sqrt{s} = 5.02 \text{ TeV}$ integrated in $2 < p_T < 8 \text{ GeV}/c$ is 0.21 ± 0.04 (stat.) ± 0.07 (syst.), which is calculated as the ratio of the integrated cross sections of Ξ_c^0 and D^0 in the considered p_T interval.

4.1 Comparison with model calculations

The left panel of figure 6 shows the comparison of the p_T -differential production cross section of Ξ_c^0 baryons with predictions from different tunes of the PYTHIA 8.243 generator, including the Monash tune [28], and tunes that implement CR beyond the leading-colour approximation [31]. In the PYTHIA 8 simulations, all soft QCD processes are enabled. In the Monash tune, the parameters governing the heavy-quark fragmentation are tuned on measurements in e^+e^- collisions. The Monash tune significantly underestimates the Ξ_c^0 -baryon production cross section by a factor of about 23 in the lowest p_T interval of the measurement and around a factor 5 in the highest p_T interval. This provides an additional information on the non-universality of charm fragmentation that was reported in refs. [17, 19, 26] based on the different baryon-to-meson ratios in e^+e^- and pp collisions and on the consideration that event generators tuned on e^+e^- data do not describe the baryon cross sections measured in pp collisions at LHC energies. The CR tunes introduce new colour reconnection topologies, including ‘‘junctions’’, which favour baryon formation. The three considered tunes (Mode 0, 2, and 3) apply different constraints on the allowed reconnection, taking into account causal connection of dipoles involved in a reconnection and time dilation effects caused by relative boosts between string pieces. It is noted that Mode 2 is recommended in ref. [31] as the standard tune, and contains the strictest constraints on the allowed reconnection. The three CR modes yield similar Ξ_c^0 p_T -differential cross sections, and predict a significantly larger Ξ_c^0 production cross section with respect to the Monash tune. However, for all three CR modes, the measured Ξ_c^0 production cross section is underestimated by a factor of about 5–6 for $2 < p_T < 3 \text{ GeV}/c$, and by a factor of about 3–4 for $p_T > 6 \text{ GeV}/c$, depending on the CR mode. The production cross section of the Ξ_c^0 baryon is also compared with a model using a coalescence approach in hadronic collisions in the framework of QCM [36, 69], in which quarks with equal velocity are combined into hadrons. A free parameter, $R_{B/M}^{(c)}$, characterises the relative production of single-charm baryons to single-charm mesons and it is set to 0.425, which is tuned to reproduce the Λ_c^+/D^0 ratio measured by ALICE in pp collisions at $\sqrt{s} = 7 \text{ TeV}$ [70]. The relative abundances of the different charm-baryon species are determined by thermal weights. The QCM model is closer to the data as compared to PYTHIA 8 with CR tunes, however it underpredicts the measured cross section by a factor 2–3 for $p_T < 4 \text{ GeV}/c$.

The measured Ξ_c^0/D^0 ratio is compared in the right panel of figure 6 with the different tunes of the PYTHIA 8 event generator previously described. All PYTHIA 8 tunes underestimate the measured p_T -differential Ξ_c^0/D^0 ratio. The Monash tune significantly underestimates the data by a factor of about 21–24 in the low p_T region and by a factor of about 7 in the highest p_T interval, as also observed for the Λ_c^+/D^0 ratio [17]. All three CR modes yield a similar magnitude and shape of the Ξ_c^0/D^0 ratio, and despite predicting a larger baryon-to-meson ratio with respect to the Monash tune, they still underestimate

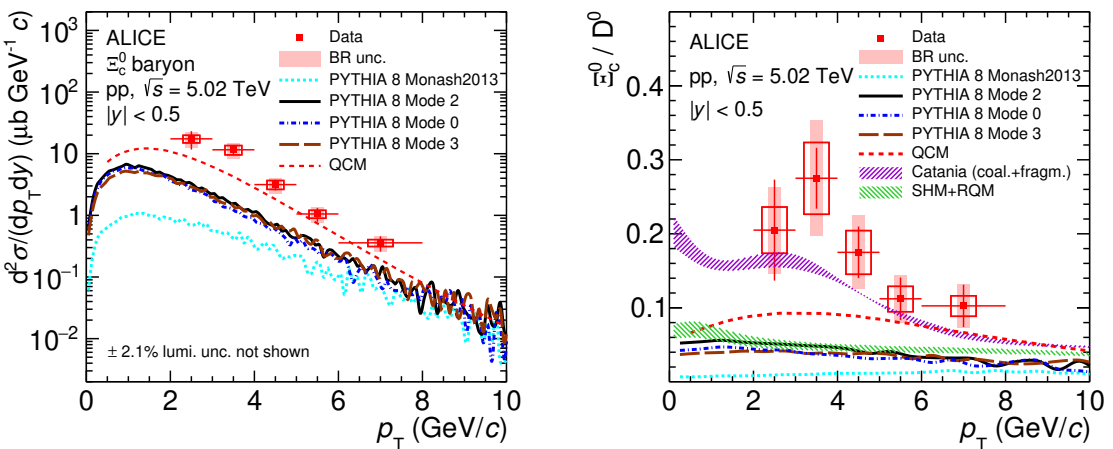


Figure 6. Left panel: p_T -differential production cross section of prompt Ξ_c^0 baryons in pp collisions at $\sqrt{s} = 5.02$ TeV compared with model calculations [28, 31, 36]. Right panel: Ξ_c^0/D^0 ratio as a function of p_T measured in pp collisions at $\sqrt{s} = 5.02$ TeV compared with model calculations [28, 31, 32, 36, 37] (see text for details).

the measured Ξ_c^0/D^0 ratio by a factor of about 4–5 at low p_T . The models with CR tunes describe better the Λ_c^+/D^0 and the $\Sigma_c^{0,+,\pm}/D^0$ ratios than the Ξ_c^0/D^0 one [9, 17, 19, 26], which involves a charm-strange baryon.

The measured Ξ_c^0/D^0 ratio is also compared with a SHM calculation [32] in which additional excited charm-baryon states not yet observed are included. The additional states are added based on the relativistic quark model (RQM) [34] and lattice QCD calculations [35]. Charm- and strange-quark fugacity factors are used in the model to account for the suppression of quarks heavier than u and d in elementary collisions. The uncertainty band in the model is obtained by varying the assumption of the branching ratios of excited charm-baryon states decaying to the ground state $\Xi_c^{0,+}$, where an exact isospin symmetry between Ξ_c^+ and Ξ_c^0 is assumed. This model, which was observed to describe the Λ_c^+/D^0 ratio [17], underestimates the measured Ξ_c^0/D^0 ratio by the same amount as PYTHIA 8 with CR tunes.

The QCM model [36] underpredicts the Ξ_c^0/D^0 ratio by the same amount as it does for the Ξ_c^0 -baryon production cross section. The Catania model [37, 46] implements charm-quark hadronisation via both coalescence and fragmentation. In the model a blast wave parametrisation [71] for light quarks at the hadronisation time with the inclusion of a contribution from mini-jets is considered, while for charm quarks the spectra from FONLL calculations are used. The coalescence process of heavy quarks with light quarks, which is modelled using the Wigner function formalism, is tuned to have all charm quarks hadronising via coalescence at $p_T \simeq 0$. At finite p_T , charm quarks not undergoing coalescence are hadronised via an independent fragmentation. The Catania model describes the Ξ_c^0/D^0 ratio in the full p_T interval of the measurement.

This new Ξ_c^0 measurement therefore provides important constraints to models of charm quark hadronisation in pp collisions, being in particular sensitive to the description of charm-strange baryon production in the colour reconnection approach, and to the possible contribution of coalescence to charm quark hadronisation in pp collisions.

4.2 Extrapolation down to $p_T = 0$ of the Ξ_c^0 cross section and the Ξ_c^0/D^0 ratio

The p_T -integrated production cross section of prompt Ξ_c^0 baryons at midrapidity is obtained by extrapolating the visible cross section, reported in eq. (4.1), to the full p_T range. The PYTHIA 8 generator with CR Mode 2 is used to calculate the central value of the extrapolation factor following what was done for the Λ_c^+ baryon [17]. This prediction was chosen because the PYTHIA 8 generator with CR Mode 2 describes the p_T shape of the measured cross section of Ξ_c^0 better than the other models that provide predictions of Ξ_c^0 production in the full p_T range. The p_T -differential Ξ_c^0 cross section values for $0 < p_T < 2 \text{ GeV}/c$ and for $p_T > 8 \text{ GeV}/c$ are obtained by multiplying the measured Ξ_c^0 cross section in $2 < p_T < 8 \text{ GeV}/c$ by the ratio of the cross sections obtained with PYTHIA 8 in the full and in the measured p_T range. The systematic uncertainty is estimated from the difference with respect to the extrapolation factors obtained using all the other available model calculations [31, 32, 36, 37] except for the Monash tune [28], which fails to reproduce the p_T shape of the Ξ_c^0 -baryon cross section. The extrapolation factor is $2.65^{+0.54}_{-0.44}$. The resulting p_T -integrated cross section of prompt Ξ_c^0 -baryon production in pp collisions at $\sqrt{s} = 5.02 \text{ TeV}$ is

$$\frac{d\sigma_{\text{pp}, 5.02 \text{ TeV}}^{\Xi_c^0}}{dy} \Big|_{|y|<0.5} = 89.8 \pm 16.0 \text{ (stat.)} \pm 28.1 \text{ (syst.)} \pm 1.9 \text{ (lumi.)}^{+18.2}_{-15.0} \text{ (extrap.)} \mu\text{b.} \quad (4.2)$$

The p_T -integrated cross section is used to calculate the ratio to the one of the D^0 meson which is measured at the same collision energy [9]. The p_T -integrated Ξ_c^0/D^0 ratio is $0.20 \pm 0.04 \text{ (stat.)}^{+0.08}_{-0.07} \text{ (syst.)}$. In the baryon-to-meson ratio the tracking, the FONLL contribution to the feed-down, and the luminosity components of the systematic uncertainty are considered as correlated between the Ξ_c^0 and the D^0 cross sections, while the other sources are treated as uncorrelated. The extrapolation uncertainty is included in the total systematic uncertainty. For an accurate measurement of the $c\bar{c}$ production cross section at midrapidity in pp collisions at the LHC, it is therefore necessary to include the large yield of Ξ_c^0 baryons.

5 Summary and conclusions

The measurement of the production of prompt Ξ_c^0 baryons in pp collisions at $\sqrt{s} = 5.02 \text{ TeV}$ at midrapidity ($|y| < 0.5$) with the ALICE detector at the LHC is reported. The analysis was performed via the semileptonic decay channel $\Xi_c^0 \rightarrow e^+ \Xi^- \nu_e$ and its charge conjugate. The p_T -differential cross section was measured in the transverse-momentum interval $2 < p_T < 8 \text{ GeV}/c$.

The measured p_T -differential cross section and Ξ_c^0/D^0 ratio were compared with different tunes of the PYTHIA 8 event generator that implement different particle production and hadronisation mechanisms. The predictions from the default PYTHIA 8 tune (Monash

2013) and from CR tunes utilising string formation beyond the leading-colour approximation are systematically lower than the experimental measurement. The PYTHIA 8 simulations with the colour-reconnection mechanism predict an enhanced production of baryons and are closer to the data, as compared to the simulation with the Monash tune. The p_T -differential Ξ_c^0/D^0 ratio was also compared with the statistical hadronisation model, which underestimates the measured ratio also in the case in which the calculations are performed assuming the existence of a large set of yet-unobserved charm-baryon states. Note that PYTHIA 8 with CR and the statistical hadronisation model with additional baryons describe reasonably well the Λ_c^+/D^0 ratio. The measured Ξ_c^0/D^0 ratio is better described by the Catania model, which implements a possible new scenario for pp collisions at LHC energies allowing low- p_T charm quarks to hadronise also via coalescence in addition to the fragmentation mechanism.

The measurements reported in this article provide an additional information of non-universality of charm fragmentation and set important and stringent constraints on models of charm-quark hadronisation in pp collisions.

Acknowledgments

The ALICE Collaboration would like to thank all its engineers and technicians for their invaluable contributions to the construction of the experiment and the CERN accelerator teams for the outstanding performance of the LHC complex. The ALICE Collaboration gratefully acknowledges the resources and support provided by all Grid centres and the Worldwide LHC Computing Grid (WLCG) collaboration. The ALICE Collaboration acknowledges the following funding agencies for their support in building and running the ALICE detector: A. I. Alikhanyan National Science Laboratory (Yerevan Physics Institute) Foundation (ANSL), State Committee of Science and World Federation of Scientists (WFS), Armenia; Austrian Academy of Sciences, Austrian Science Fund (FWF): [M 2467-N36] and Nationalstiftung für Forschung, Technologie und Entwicklung, Austria; Ministry of Communications and High Technologies, National Nuclear Research Center, Azerbaijan; Conselho Nacional de Desenvolvimento Científico e Tecnológico (CNPq), Financiadora de Estudos e Projetos (Finep), Fundação de Amparo à Pesquisa do Estado de São Paulo (FAPESP) and Universidade Federal do Rio Grande do Sul (UFRGS), Brazil; Ministry of Education of China (MOEC), Ministry of Science & Technology of China (MSTC) and National Natural Science Foundation of China (NSFC), China; Ministry of Science and Education and Croatian Science Foundation, Croatia; Centro de Aplicaciones Tecnológicas y Desarrollo Nuclear (CEADEN), Cubaenergía, Cuba; Ministry of Education, Youth and Sports of the Czech Republic, Czech Republic; The Danish Council for Independent Research | Natural Sciences, the VILLUM FONDEN and Danish National Research Foundation (DNRF), Denmark; Helsinki Institute of Physics (HIP), Finland; Commissariat à l’Energie Atomique (CEA) and Institut National de Physique Nucléaire et de Physique des Particules (IN2P3) and Centre National de la Recherche Scientifique (CNRS), France; Bundesministerium für Bildung und Forschung (BMBF) and GSI Helmholtzzentrum für Schwerionenforschung GmbH, Germany; General Secretariat for Research and Technol-

ogy, Ministry of Education, Research and Religions, Greece; National Research, Development and Innovation Office, Hungary; Department of Atomic Energy Government of India (DAE), Department of Science and Technology, Government of India (DST), University Grants Commission, Government of India (UGC) and Council of Scientific and Industrial Research (CSIR), India; Indonesian Institute of Science, Indonesia; Istituto Nazionale di Fisica Nucleare (INFN), Italy; Institute for Innovative Science and Technology, Nagasaki Institute of Applied Science (IIST), Japanese Ministry of Education, Culture, Sports, Science and Technology (MEXT) and Japan Society for the Promotion of Science (JSPS) KAKENHI, Japan; Consejo Nacional de Ciencia (CONACYT) y Tecnología, through Fondo de Cooperación Internacional en Ciencia y Tecnología (FONCICYT) and Dirección General de Asuntos del Personal Académico (DGAPA), Mexico; Nederlandse Organisatie voor Wetenschappelijk Onderzoek (NWO), Netherlands; The Research Council of Norway, Norway; Commission on Science and Technology for Sustainable Development in the South (COMSATS), Pakistan; Pontificia Universidad Católica del Perú, Peru; Ministry of Education and Science, National Science Centre and WUT ID-UB, Poland; Korea Institute of Science and Technology Information and National Research Foundation of Korea (NRF), Republic of Korea; Ministry of Education and Scientific Research, Institute of Atomic Physics and Ministry of Research and Innovation and Institute of Atomic Physics, Romania; Joint Institute for Nuclear Research (JINR), Ministry of Education and Science of the Russian Federation, National Research Centre Kurchatov Institute, Russian Science Foundation and Russian Foundation for Basic Research, Russia; Ministry of Education, Science, Research and Sport of the Slovak Republic, Slovakia; National Research Foundation of South Africa, South Africa; Swedish Research Council (VR) and Knut & Alice Wallenberg Foundation (KAW), Sweden; European Organization for Nuclear Research, Switzerland; Suranaree University of Technology (SUT), National Science and Technology Development Agency (NSDTA) and Office of the Higher Education Commission under NRU project of Thailand, Thailand; Turkish Energy, Nuclear and Mineral Research Agency (TENMAK), Turkey; National Academy of Sciences of Ukraine, Ukraine; Science and Technology Facilities Council (STFC), United Kingdom; National Science Foundation of the United States of America (NSF) and United States Department of Energy, Office of Nuclear Physics (DOE NP), United States of America.

Open Access. This article is distributed under the terms of the Creative Commons Attribution License ([CC-BY 4.0](#)), which permits any use, distribution and reproduction in any medium, provided the original author(s) and source are credited.

References

- [1] J.C. Collins, D.E. Soper and G.F. Sterman, *Heavy particle production in high-energy hadron collisions*, *Nucl. Phys. B* **263** (1986) 37 [[INSPIRE](#)].
- [2] ALICE collaboration, *Measurement of D^0 , D^+ , D^{*+} and D_s^+ production in pp collisions at $\sqrt{s} = 5.02$ TeV with ALICE*, *Eur. Phys. J. C* **79** (2019) 388 [[arXiv:1901.07979](#)] [[INSPIRE](#)].
- [3] ALICE collaboration, *Measurement of D-meson production at mid-rapidity in pp collisions at $\sqrt{s} = 7$ TeV*, *Eur. Phys. J. C* **77** (2017) 550 [[arXiv:1702.00766](#)] [[INSPIRE](#)].

- [4] ALICE collaboration, *Measurement of charm production at central rapidity in proton-proton collisions at $\sqrt{s} = 2.76$ TeV*, *JHEP* **07** (2012) 191 [[arXiv:1205.4007](#)] [[INSPIRE](#)].
- [5] CMS collaboration, *Nuclear modification factor of D^0 mesons in PbPb collisions at $\sqrt{s_{NN}} = 5.02$ TeV*, *Phys. Lett. B* **782** (2018) 474 [[arXiv:1708.04962](#)] [[INSPIRE](#)].
- [6] CMS collaboration, *Measurement of the B^+ production cross section in pp collisions at $\sqrt{s} = 7$ TeV*, *Phys. Rev. Lett.* **106** (2011) 112001 [[arXiv:1101.0131](#)] [[INSPIRE](#)].
- [7] CMS collaboration, *Measurement of the B^0 production cross section in pp collisions at $\sqrt{s} = 7$ TeV*, *Phys. Rev. Lett.* **106** (2011) 252001 [[arXiv:1104.2892](#)] [[INSPIRE](#)].
- [8] CMS collaboration, *Measurement of the strange B meson production cross section with $J/\Psi \phi$ decays in pp collisions at $\sqrt{s} = 7$ TeV*, *Phys. Rev. D* **84** (2011) 052008 [[arXiv:1106.4048](#)] [[INSPIRE](#)].
- [9] ALICE collaboration, *Measurement of beauty and charm production in pp collisions at $\sqrt{s} = 5.02$ TeV via non-prompt and prompt D mesons*, *JHEP* **05** (2021) 220 [[arXiv:2102.13601](#)] [[INSPIRE](#)].
- [10] G. Kramer and H. Spiesberger, *Study of heavy meson production in p-Pb collisions at $\sqrt{s} = 5.02$ TeV in the general-mass variable-flavour-number scheme*, *Nucl. Phys. B* **925** (2017) 415 [[arXiv:1703.04754](#)] [[INSPIRE](#)].
- [11] I. Helenius and H. Paukkunen, *Revisiting the D -meson hadroproduction in general-mass variable flavour number scheme*, *JHEP* **05** (2018) 196 [[arXiv:1804.03557](#)] [[INSPIRE](#)].
- [12] B.A. Kniehl, G. Kramer, I. Schienbein and H. Spiesberger, *Λ_c^\pm production in pp collisions with a new fragmentation function*, *Phys. Rev. D* **101** (2020) 114021 [[arXiv:2004.04213](#)] [[INSPIRE](#)].
- [13] M. Cacciari, M. Greco and P. Nason, *The p_T spectrum in heavy flavor hadroproduction*, *JHEP* **05** (1998) 007 [[hep-ph/9803400](#)] [[INSPIRE](#)].
- [14] M. Cacciari, S. Frixione, N. Houdeau, M.L. Mangano, P. Nason and G. Ridolfi, *Theoretical predictions for charm and bottom production at the LHC*, *JHEP* **10** (2012) 137 [[arXiv:1205.6344](#)] [[INSPIRE](#)].
- [15] CMS collaboration, *Production of Λ_c^+ baryons in proton-proton and lead-lead collisions at $\sqrt{s_{NN}} = 5.02$ TeV*, *Phys. Lett. B* **803** (2020) 135328 [[arXiv:1906.03322](#)] [[INSPIRE](#)].
- [16] ALICE collaboration, *Λ_c^+ production in pp collisions at $\sqrt{s} = 7$ TeV and in p-Pb collisions at $\sqrt{s_{NN}} = 5.02$ TeV*, *JHEP* **04** (2018) 108 [[arXiv:1712.09581](#)] [[INSPIRE](#)].
- [17] ALICE collaboration, *Λ_c^+ production and baryon-to-meson ratios in pp and p-Pb collisions at $\sqrt{s_{NN}} = 5.02$ TeV at the LHC*, [arXiv:2011.06078](#) [[INSPIRE](#)].
- [18] ALICE collaboration, *Λ_c^+ production in pp and in p-Pb collisions at $\sqrt{s_{NN}} = 5.02$ TeV*, [arXiv:2011.06079](#) [[INSPIRE](#)].
- [19] ALICE collaboration, *Measurement of prompt D^0 , Λ_c^+ , and $\Sigma_c^{0,++}(2455)$ production in pp collisions at $\sqrt{s} = 13$ TeV*, [arXiv:2106.08278](#) [[INSPIRE](#)].
- [20] ARGUS collaboration, *Observation of the charmed baryon Λ_c in e^+e^- annihilation at 10 GeV*, *Phys. Lett. B* **207** (1988) 109 [[INSPIRE](#)].
- [21] CLEO collaboration, *Inclusive production of the charmed baryon Λ_c from e^+e^- annihilations at $\sqrt{s} = 10.55$ GeV*, *Phys. Rev. D* **43** (1991) 3599 [[INSPIRE](#)].

- [22] L. Gladilin, *Fragmentation fractions of c and b quarks into charmed hadrons at LEP*, *Eur. Phys. J. C* **75** (2015) 19 [[arXiv:1404.3888](#)] [[INSPIRE](#)].
- [23] ZEUS collaboration, *Measurement of charm fragmentation ratios and fractions in photoproduction at HERA*, *Eur. Phys. J. C* **44** (2005) 351 [[hep-ex/0508019](#)] [[INSPIRE](#)].
- [24] ZEUS collaboration, *Measurement of charm fragmentation fractions in photoproduction at HERA*, *JHEP* **09** (2013) 058 [[arXiv:1306.4862](#)] [[INSPIRE](#)].
- [25] ALICE collaboration, *First measurement of Ξ_c^0 production in pp collisions at $\sqrt{s} = 7$ TeV*, *Phys. Lett. B* **781** (2018) 8 [[arXiv:1712.04242](#)] [[INSPIRE](#)].
- [26] ALICE collaboration, *Measurement of the cross sections of Ξ_c^0 and Ξ_c^+ baryons and branching-fraction ratio $BR(\Xi_c^0 \rightarrow \Xi^- e^+ \nu_e)/BR(\Xi_c^0 \rightarrow \Xi^- \pi^+)$ in pp collisions at 13 TeV*, [arXiv:2105.05187](#) [[INSPIRE](#)].
- [27] S. Frixione, P. Nason and G. Ridolfi, *A positive-weight next-to-leading-order Monte Carlo for heavy flavour hadroproduction*, *JHEP* **09** (2007) 126 [[arXiv:0707.3088](#)] [[INSPIRE](#)].
- [28] P. Skands, S. Carrazza and J. Rojo, *Tuning PYTHIA 8.1: the Monash 2013 tune*, *Eur. Phys. J. C* **74** (2014) 3024 [[arXiv:1404.5630](#)] [[INSPIRE](#)].
- [29] C. Bierlich and J.R. Christiansen, *Effects of color reconnection on hadron flavor observables*, *Phys. Rev. D* **92** (2015) 094010 [[arXiv:1507.02091](#)] [[INSPIRE](#)].
- [30] M. Bahr et al., *HERWIG++ physics and manual*, *Eur. Phys. J. C* **58** (2008) 639 [[arXiv:0803.0883](#)] [[INSPIRE](#)].
- [31] J.R. Christiansen and P.Z. Skands, *String formation beyond leading colour*, *JHEP* **08** (2015) 003 [[arXiv:1505.01681](#)] [[INSPIRE](#)].
- [32] M. He and R. Rapp, *Charm-baryon production in proton-proton collisions*, *Phys. Lett. B* **795** (2019) 117 [[arXiv:1902.08889](#)] [[INSPIRE](#)].
- [33] PARTICLE DATA GROUP collaboration, *Review of particle physics*, *PTEP* **2020** (2020) 083C01 [[INSPIRE](#)].
- [34] D. Ebert, R.N. Faustov and V.O. Galkin, *Spectroscopy and Regge trajectories of heavy baryons in the relativistic quark-diquark picture*, *Phys. Rev. D* **84** (2011) 014025 [[arXiv:1105.0583](#)] [[INSPIRE](#)].
- [35] R.A. Briceno, H.-W. Lin and D.R. Bolton, *Charmed-baryon spectroscopy from lattice QCD with $N_f = 2 + 1 + 1$ flavors*, *Phys. Rev. D* **86** (2012) 094504 [[arXiv:1207.3536](#)] [[INSPIRE](#)].
- [36] J. Song, H.-H. Li and F.-L. Shao, *New feature of low p_T charm quark hadronization in pp collisions at $\sqrt{s} = 7$ TeV*, *Eur. Phys. J. C* **78** (2018) 344 [[arXiv:1801.09402](#)] [[INSPIRE](#)].
- [37] V. Minissale, S. Plumari and V. Greco, *Charm hadrons in pp collisions at LHC energy within a coalescence plus fragmentation approach*, *Phys. Lett. B* **821** (2021) 136622 [[arXiv:2012.12001](#)] [[INSPIRE](#)].
- [38] C.B. Dover, U.W. Heinz, E. Schnedermann and J. Zimanyi, *Relativistic coalescence model for high-energy nuclear collisions*, *Phys. Rev. C* **44** (1991) 1636 [[INSPIRE](#)].
- [39] ALICE collaboration, *J/ψ suppression at forward rapidity in Pb-Pb collisions at $\sqrt{s_{NN}} = 5.02$ TeV*, *Phys. Lett. B* **766** (2017) 212 [[arXiv:1606.08197](#)] [[INSPIRE](#)].
- [40] ALICE collaboration, *Centrality and transverse momentum dependence of inclusive J/ψ production at midrapidity in Pb-Pb collisions at $\sqrt{s_{NN}} = 5.02$ TeV*, *Phys. Lett. B* **805** (2020) 135434 [[arXiv:1910.14404](#)] [[INSPIRE](#)].

- [41] A. Andronic, P. Braun-Munzinger, M.K. Köhler, K. Redlich and J. Stachel, *Transverse momentum distributions of charmonium states with the statistical hadronization model*, *Phys. Lett. B* **797** (2019) 134836 [[arXiv:1901.09200](#)] [[INSPIRE](#)].
- [42] X. Zhao and R. Rapp, *Medium modifications and production of charmonia at LHC*, *Nucl. Phys. A* **859** (2011) 114 [[arXiv:1102.2194](#)] [[INSPIRE](#)].
- [43] Y.-P. Liu, Z. Qu, N. Xu and P.-F. Zhuang, *J/ψ transverse momentum distribution in high energy nuclear collisions at RHIC*, *Phys. Lett. B* **678** (2009) 72 [[arXiv:0901.2757](#)] [[INSPIRE](#)].
- [44] S.H. Lee, K. Ohnishi, S. Yasui, I.-K. Yoo and C.-M. Ko, Λ_c enhancement from strongly coupled quark-gluon plasma, *Phys. Rev. Lett.* **100** (2008) 222301 [[arXiv:0709.3637](#)] [[INSPIRE](#)].
- [45] Y. Oh, C.M. Ko, S.H. Lee and S. Yasui, *Heavy baryon/meson ratios in relativistic heavy ion collisions*, *Phys. Rev. C* **79** (2009) 044905 [[arXiv:0901.1382](#)] [[INSPIRE](#)].
- [46] S. Plumari, V. Minissale, S.K. Das, G. Coci and V. Greco, *Charmed hadrons from coalescence plus fragmentation in relativistic nucleus-nucleus collisions at RHIC and LHC*, *Eur. Phys. J. C* **78** (2018) 348 [[arXiv:1712.00730](#)] [[INSPIRE](#)].
- [47] ALICE collaboration, *The ALICE experiment at the CERN LHC*, 2008 *JINST* **3** S08002 [[INSPIRE](#)].
- [48] ALICE collaboration, *Performance of the ALICE experiment at the CERN LHC*, *Int. J. Mod. Phys. A* **29** (2014) 1430044 [[arXiv:1402.4476](#)] [[INSPIRE](#)].
- [49] ALICE collaboration, *Alignment of the ALICE inner tracking system with cosmic-ray tracks*, 2010 *JINST* **5** P03003 [[arXiv:1001.0502](#)] [[INSPIRE](#)].
- [50] J. Alme et al., *The ALICE TPC, a large 3-dimensional tracking device with fast readout for ultra-high multiplicity events*, *Nucl. Instrum. Meth. A* **622** (2010) 316 [[arXiv:1001.1950](#)] [[INSPIRE](#)].
- [51] A. Akindinov et al., *Performance of the ALICE time-of-flight detector at the LHC*, *Eur. Phys. J. Plus* **128** (2013) 44.
- [52] M. Bondila et al., *ALICE T0 detector*, *IEEE Trans. Nucl. Sci.* **52** (2005) 1705.
- [53] ALICE collaboration, *Performance of the ALICE VZERO system*, 2013 *JINST* **8** P10016 [[arXiv:1306.3130](#)] [[INSPIRE](#)].
- [54] ALICE collaboration, *ALICE 2017 luminosity determination for pp collisions at $\sqrt{s} = 5 \text{ TeV}$* , [ALICE-PUBLIC-2018-014](#), CERN, Geneva, Switzerland (2018).
- [55] LHCb collaboration, *Measurement of b hadron fractions in 13 TeV pp collisions*, *Phys. Rev. D* **100** (2019) 031102 [[arXiv:1902.06794](#)] [[INSPIRE](#)].
- [56] ALICE collaboration, *Measurements of low- p_T electrons from semileptonic heavy-flavour hadron decays at mid-rapidity in pp and Pb-Pb collisions at $\sqrt{s_{NN}} = 2.76 \text{ TeV}$* , *JHEP* **10** (2018) 061 [[arXiv:1805.04379](#)] [[INSPIRE](#)].
- [57] ALICE collaboration, *Measurement of electrons from semileptonic heavy-flavour hadron decays at midrapidity in pp and Pb-Pb collisions at $\sqrt{s_{NN}} = 5.02 \text{ TeV}$* , *Phys. Lett. B* **804** (2020) 135377 [[arXiv:1910.09110](#)] [[INSPIRE](#)].
- [58] ALICE collaboration, *Inclusive J/ψ production at mid-rapidity in pp collisions at $\sqrt{s} = 5.02 \text{ TeV}$* , *JHEP* **10** (2019) 084 [[arXiv:1905.07211](#)] [[INSPIRE](#)].

- [59] ALICE collaboration, *Measurement of electrons from heavy-flavour hadron decays in p-Pb collisions at $\sqrt{s_{NN}} = 5.02$ TeV*, *Phys. Lett. B* **754** (2016) 81 [[arXiv:1509.07491](#)] [[INSPIRE](#)].
- [60] ALICE collaboration, *Multiplicity dependence of (multi-)strange hadron production in proton-proton collisions at $\sqrt{s} = 13$ TeV*, *Eur. Phys. J. C* **80** (2020) 167 [[arXiv:1908.01861](#)] [[INSPIRE](#)].
- [61] CMS collaboration, *Measurement of the Λ_b cross section and the $\bar{\Lambda}_b$ to Λ_b ratio with $J/\Psi\Lambda$ decays in pp collisions at $\sqrt{s} = 7$ TeV*, *Phys. Lett. B* **714** (2012) 136 [[arXiv:1205.0594](#)] [[INSPIRE](#)].
- [62] ALEPH collaboration, *Measurement of the B baryon lifetime and branching fractions in Z decays*, *Eur. Phys. J. C* **2** (1998) 197 [[INSPIRE](#)].
- [63] T. Sjöstrand et al., *An introduction to PYTHIA 8.2*, *Comput. Phys. Commun.* **191** (2015) 159 [[arXiv:1410.3012](#)] [[INSPIRE](#)].
- [64] R. Brun et al., *GEANT: detector description and simulation tool*, CERN Program Library, CERN, Geneva, Switzerland (1993).
- [65] G. D'Agostini, *A multidimensional unfolding method based on Bayes' theorem*, *Nucl. Instrum. Meth. A* **362** (1995) 487 [[INSPIRE](#)].
- [66] T. Adye, *Unfolding algorithms and tests using RooUnfold*, in *PHYSTAT 2011*, CERN-2011-006, CERN, Geneva, Switzerland (2011), pg. 313 [[arXiv:1105.1160](#)] [[INSPIRE](#)].
- [67] A. Hocker and V. Kartvelishvili, *SVD approach to data unfolding*, *Nucl. Instrum. Meth. A* **372** (1996) 469 [[hep-ph/9509307](#)] [[INSPIRE](#)].
- [68] LHCb collaboration, *Measurement of the mass and production rate of Ξ_b^- baryons*, *Phys. Rev. D* **99** (2019) 052006 [[arXiv:1901.07075](#)] [[INSPIRE](#)].
- [69] X.-R. Gou, F.-L. Shao, R.-Q. Wang, H.-H. Li and J. Song, *New insights into hadron production mechanism from p_T spectra in pp collisions at $\sqrt{s} = 7$ TeV*, *Phys. Rev. D* **96** (2017) 094010 [[arXiv:1707.06906](#)] [[INSPIRE](#)].
- [70] H.-H. Li, F.-L. Shao, J. Song and R.-Q. Wang, *Production of single-charm hadrons by quark combination mechanism in p-Pb collisions at $\sqrt{s_{NN}} = 5.02$ TeV*, *Phys. Rev. C* **97** (2018) 064915 [[arXiv:1712.08921](#)] [[INSPIRE](#)].
- [71] F. Retiere and M.A. Lisa, *Observable implications of geometrical and dynamical aspects of freeze out in heavy ion collisions*, *Phys. Rev. C* **70** (2004) 044907 [[nucl-th/0312024](#)] [[INSPIRE](#)].

The ALICE collaboration

S. Acharya¹⁴³, D. Adamová⁹⁸, A. Adler⁷⁶, J. Adolfsson⁸³, G. Aglieri Rinella³⁵, M. Agnello³¹, N. Agrawal⁵⁵, Z. Ahammed¹⁴³, S. Ahmad¹⁶, S.U. Ahn⁷⁸, I. Ahuja³⁹, Z. Akbar⁵², A. Akindinov⁹⁵, M. Al-Turany¹¹⁰, S.N. Alam⁴¹, D. Aleksandrov⁹¹, B. Alessandro⁶¹, H.M. Alfanda⁷, R. Alfaro Molina⁷³, B. Ali¹⁶, Y. Ali¹⁴, A. Alici²⁶, N. Alizadehvandchali¹²⁷, A. Alkin³⁵, J. Alme²¹, T. Alt⁷⁰, L. Altenkamper²¹, I. Altsybeev¹¹⁵, M.N. Anaam⁷, C. Andrei⁴⁹, D. Andreou⁹³, A. Andronic¹⁴⁶, M. Angeletti³⁵, V. Anguelov¹⁰⁷, F. Antinori⁵⁸, P. Antonioli⁵⁵, C. Anuj¹⁶, N. Apadula⁸², L. Aphecetche¹¹⁷, H. Appelshäuser⁷⁰, S. Arcelli²⁶, R. Arnaldi⁶¹, I.C. Arsene²⁰, M. Arslanbekov^{148,107}, A. Augustinus³⁵, R. Averbeck¹¹⁰, S. Aziz⁸⁰, M.D. Azmi¹⁶, A. Badalà⁵⁷, Y.W. Baek⁴², X. Bai^{131,110}, R. Bailhache⁷⁰, Y. Bailung⁵¹, R. Bala¹⁰⁴, A. Balbino³¹, A. Baldissari¹⁴⁰, B. Balis², M. Ball⁴⁴, D. Banerjee⁴, R. Barbera²⁷, L. Barioglio^{108,25}, M. Barlou⁸⁷, G.G. Barnaföldi¹⁴⁷, L.S. Barnby⁹⁷, V. Barret¹³⁷, C. Bartels¹³⁰, K. Barth³⁵, E. Bartsch⁷⁰, F. Baruffaldi²⁸, N. Bastid¹³⁷, S. Basu⁸³, G. Batigne¹¹⁷, B. Batyunya⁷⁷, D. Bauri⁵⁰, J.L. Bazo Alba¹¹⁴, I.G. Bearden⁹², C. Beattie¹⁴⁸, I. Belikov¹³⁹, A.D.C. Bell Hechavarria¹⁴⁶, F. Bellini^{26,35}, R. Bellwied¹²⁷, S. Belokurova¹¹⁵, V. Belyaev⁹⁶, G. Bencedi⁷¹, S. Beole²⁵, A. Bercuci⁴⁹, Y. Berdnikov¹⁰¹, A. Berdnikova¹⁰⁷, D. Berenyi¹⁴⁷, L. Bergmann¹⁰⁷, M.G. Besoiu⁶⁹, L. Betev³⁵, P.P. Bhaduri¹⁴³, A. Bhasin¹⁰⁴, I.R. Bhat¹⁰⁴, M.A. Bhat⁴, B. Bhattacharjee⁴³, P. Bhattacharya²³, L. Bianchi²⁵, N. Bianchi⁵³, J. Bielčík³⁸, J. Bielčíková⁹⁸, J. Biernat¹²⁰, A. Bilandzic¹⁰⁸, G. Biro¹⁴⁷, S. Biswas⁴, J.T. Blair¹²¹, D. Blau⁹¹, M.B. Blidaru¹¹⁰, C. Blume⁷⁰, G. Boca^{29,59}, F. Bock⁹⁹, A. Bogdanov⁹⁶, S. Boi²³, J. Bok⁶³, L. Boldizsár¹⁴⁷, A. Bolozdynya⁹⁶, M. Bomba³⁹, P.M. Bond³⁵, G. Bonomi^{142,59}, H. Borel¹⁴⁰, A. Borissov⁸⁴, H. Bossi¹⁴⁸, E. Botta²⁵, L. Bratrud⁷⁰, P. Braun-Munzinger¹¹⁰, M. Bregant¹²³, M. Broz³⁸, G.E. Bruno^{109,34}, M.D. Buckland¹³⁰, D. Budnikov¹¹¹, H. Buesching⁷⁰, S. Bufalino³¹, O. Bugnon¹¹⁷, P. Buhler¹¹⁶, Z. Buthelezi^{74,134}, J.B. Butt¹⁴, S.A. Bysiak¹²⁰, D. Caffarri⁹³, M. Cai^{28,7}, H. Caines¹⁴⁸, A. Caliva¹¹⁰, E. Calvo Villar¹¹⁴, J.M.M. Camacho¹²², R.S. Camacho⁴⁶, P. Camerini²⁴, F.D.M. Canedo¹²³, F. Carnesecchi^{35,26}, R. Caron¹⁴⁰, J. Castillo Castellanos¹⁴⁰, E.A.R. Casula²³, F. Catalano³¹, C. Ceballos Sanchez⁷⁷, P. Chakraborty⁵⁰, S. Chandra¹⁴³, S. Chapelard³⁵, M. Chartier¹³⁰, S. Chattopadhyay¹⁴³, S. Chattopadhyay¹¹², A. Chauvin²³, T.G. Chavez⁴⁶, T. Cheng⁷, C. Cheshkov¹³⁸, B. Cheynis¹³⁸, V. Chibante Barroso³⁵, D.D. Chinellato¹²⁴, S. Cho⁶³, P. Chochula³⁵, P. Christakoglou⁹³, C.H. Christensen⁹², P. Christiansen⁸³, T. Chujo¹³⁶, C. Cicalo⁵⁶, L. Cifarelli²⁶, F. Cindolo⁵⁵, M.R. Ciupek¹¹⁰, G. Clai^{II,55}, J. Cleymans^{I,126}, F. Colamaria⁵⁴, J.S. Colburn¹¹³, D. Colella^{109,54,34,147}, A. Collu⁸², M. Colocci^{35,26}, M. Concas^{III,61}, G. Conesa Balbastre⁸¹, Z. Conesa del Valle⁸⁰, G. Contin²⁴, J.G. Contreras³⁸, M.L. Coquet¹⁴⁰, T.M. Cormier⁹⁹, P. Cortese³², M.R. Cosentino¹²⁵, F. Costa³⁵, S. Costanza^{29,59}, P. Crochet¹³⁷, R. Cruz-Torres⁸², E. Cuautle⁷¹, P. Cui⁷, L. Cunqueiro⁹⁹, A. Dainese⁵⁸, F.P.A. Damas^{117,140}, M.C. Danisch¹⁰⁷, A. Danu⁶⁹, I. Das¹¹², P. Das⁸⁹, P. Das⁴, S. Das⁴, S. Dash⁵⁰, S. De⁸⁹, A. De Caro³⁰, G. de Cataldo⁵⁴, L. De Cilladi²⁵, J. de Cuveland⁴⁰, A. De Falco²³, D. De Gruttola³⁰, N. De Marco⁶¹, C. De Martin²⁴, S. De Pasquale³⁰, S. Deb⁵¹, H.F. Degenhardt¹²³, K.R. Deja¹⁴⁴, L. Dello Stritto³⁰, S. Delsanto²⁵, W. Deng⁷, P. Dhankher¹⁹, D. Di Bari³⁴, A. Di Mauro³⁵, R.A. Diaz⁸, T. Dietel¹²⁶, Y. Ding^{138,7}, R. Divià³⁵, D.U. Dixit¹⁹, Ø. Djupsland²¹, U. Dmitrieva⁶⁵, J. Do⁶³, A. Dobrin⁶⁹, B. Dönigus⁷⁰, O. Dordic²⁰, A.K. Dubey¹⁴³, A. Dubla^{110,93}, S. Dudi¹⁰³, M. Dukhishyam⁸⁹, P. Dupieux¹³⁷, N. Dzalaiova¹³, T.M. Eder¹⁴⁶, R.J. Ehlers⁹⁹, V.N. Eikeland²¹, F. Eisenhut⁷⁰, D. Elia⁵⁴, B. Erazmus¹¹⁷, F. Ercolelli²⁶, F. Erhardt¹⁰², A. Erokhin¹¹⁵, M.R. Ersdal²¹, B. Espagnon⁸⁰, G. Eulisse³⁵, D. Evans¹¹³, S. Evdokimov⁹⁴, L. Fabbietti¹⁰⁸, M. Faggin²⁸, J. Faivre⁸¹, F. Fan⁷, A. Fantoni⁵³, M. Fasel⁹⁹, P. Fecchio³¹, A. Feliciello⁶¹, G. Feofilov¹¹⁵, A. Fernández Téllez⁴⁶, A. Ferrero¹⁴⁰, A. Ferretti²⁵, V.J.G. Feuillard¹⁰⁷, J. Figiel¹²⁰, S. Filchagin¹¹¹, D. Finogeev⁶⁵, F.M. Fionda^{56,21},

- G. Fiorenza^{35,109}, F. Flor¹²⁷, A.N. Flores¹²¹, S. Foertsch⁷⁴, P. Foka¹¹⁰, S. Fokin⁹¹, E. Fragiacomo⁶², E. Frajna¹⁴⁷, U. Fuchs³⁵, N. Funicello³⁰, C. Furget⁸¹, A. Furs⁶⁵, J.J. Gaardhøje⁹², M. Gagliardi²⁵, A.M. Gago¹¹⁴, A. Gal¹³⁹, C.D. Galvan¹²², P. Ganoti⁸⁷, C. Garabatos¹¹⁰, J.R.A. Garcia⁴⁶, E. Garcia-Solis¹⁰, K. Garg¹¹⁷, C. Gargiulo³⁵, A. Garibli⁹⁰, K. Garner¹⁴⁶, P. Gasik¹¹⁰, E.F. Gauger¹²¹, A. Gautam¹²⁹, M.B. Gay Ducati⁷², M. Germain¹¹⁷, J. Ghosh¹¹², P. Ghosh¹⁴³, S.K. Ghosh⁴, M. Giacalone²⁶, P. Gianotti⁵³, P. Giubellino^{110,61}, P. Giubilato²⁸, A.M.C. Glaenzer¹⁴⁰, P. Glässel¹⁰⁷, D.J.Q. Goh⁸⁵, V. Gonzalez¹⁴⁵, L.H. González-Trueba⁷³, S. Gorbunov⁴⁰, M. Gorgon², L. Görlich¹²⁰, S. Gotovac³⁶, V. Grabski⁷³, L.K. Graczykowski¹⁴⁴, L. Greiner⁸², A. Grelli⁶⁴, C. Grigoras³⁵, V. Grigoriev⁹⁶, A. Grigoryan^{I,1}, S. Grigoryan^{77,1}, O.S. Groettvik²¹, F. Grossa^{35,61}, J.F. Grosse-Oetringhaus³⁵, R. Grosso¹¹⁰, G.G. Guardiano¹²⁴, R. Guernane⁸¹, M. Guilbaud¹¹⁷, K. Gulbrandsen⁹², T. Gunji¹³⁵, A. Gupta¹⁰⁴, R. Gupta¹⁰⁴, I.B. Guzman⁴⁶, S.P. Guzman⁴⁶, L. Gyulai¹⁴⁷, M.K. Habib¹¹⁰, C. Hadjidakis⁸⁰, G. Halimoglu⁷⁰, H. Hamagaki⁸⁵, G. Hamar¹⁴⁷, M. Hamid⁷, R. Hannigan¹²¹, M.R. Haque^{144,89}, A. Harlenderova¹¹⁰, J.W. Harris¹⁴⁸, A. Harton¹⁰, J.A. Hasenbichler³⁵, H. Hassan⁹⁹, D. Hatzifotiadou⁵⁵, P. Hauer⁴⁴, L.B. Havener¹⁴⁸, S. Hayashi¹³⁵, S.T. Heckel¹⁰⁸, E. Hellbär⁷⁰, H. Helstrup³⁷, T. Herman³⁸, E.G. Hernandez⁴⁶, G. Herrera Corral⁹, F. Herrmann¹⁴⁶, K.F. Hetland³⁷, H. Hillemanns³⁵, C. Hills¹³⁰, B. Hippolyte¹³⁹, B. Hofman⁶⁴, B. Hohlweger^{93,108}, J. Honermann¹⁴⁶, G.H. Hong¹⁴⁹, D. Horak³⁸, S. Hornung¹¹⁰, A. Horzyk², R. Hosokawa¹⁵, P. Hristov³⁵, C. Huang⁸⁰, C. Hughes¹³³, P. Huhn⁷⁰, T.J. Humanic¹⁰⁰, H. Hushnud¹¹², L.A. Husova¹⁴⁶, A. Hutson¹²⁷, D. Hutter⁴⁰, J.P. Iddon^{35,130}, R. Ilkaev¹¹¹, H. Ilyas¹⁴, M. Inaba¹³⁶, G.M. Innocenti³⁵, M. Ippolitov⁹¹, A. Isakov^{38,98}, M.S. Islam¹¹², M. Ivanov¹¹⁰, V. Ivanov¹⁰¹, V. Izucheev⁹⁴, M. Jablonski², B. Jacak⁸², N. Jacazio³⁵, P.M. Jacobs⁸², S. Jadlovska¹¹⁹, J. Jadlovsky¹¹⁹, S. Jaelani⁶⁴, C. Jahnke^{124,123}, M.J. Jakubowska¹⁴⁴, M.A. Janik¹⁴⁴, T. Janson⁷⁶, M. Jercic¹⁰², O. Jevons¹¹³, F. Jonas^{99,146}, P.G. Jones¹¹³, J.M. Jowett^{35,110}, J. Jung⁷⁰, M. Jung⁷⁰, A. Junique³⁵, A. Jusko¹¹³, J. Kaewjai¹¹⁸, P. Kalinak⁶⁶, A. Kalweit³⁵, V. Kaplin⁹⁶, S. Kar⁷, A. Karasu Uysal⁷⁹, D. Karatovic¹⁰², O. Karavichev⁶⁵, T. Karavicheva⁶⁵, P. Karczmarczyk¹⁴⁴, E. Karpechev⁶⁵, A. Kazantsev⁹¹, U. Kebschull⁷⁶, R. Keidel⁴⁸, D.L.D. Keijdener⁶⁴, M. Keil³⁵, B. Ketzer⁴⁴, Z. Khabanova⁹³, A.M. Khan⁷, S. Khan¹⁶, A. Khanzadeev¹⁰¹, Y. Kharlov⁹⁴, A. Khatun¹⁶, A. Khuntia¹²⁰, B. Kileng³⁷, B. Kim^{17,63}, D. Kim¹⁴⁹, D.J. Kim¹²⁸, E.J. Kim⁷⁵, J. Kim¹⁴⁹, J.S. Kim⁴², J. Kim¹⁰⁷, J. Kim¹⁴⁹, J. Kim⁷⁵, M. Kim¹⁰⁷, S. Kim¹⁸, T. Kim¹⁴⁹, S. Kirsch⁷⁰, I. Kisel⁴⁰, S. Kiselev⁹⁵, A. Kisiel¹⁴⁴, J.P. Kitowski², J.L. Klay⁶, J. Klein³⁵, S. Klein⁸², C. Klein-Bösing¹⁴⁶, M. Kleiner⁷⁰, T. Klemenz¹⁰⁸, A. Kluge³⁵, A.G. Knospe¹²⁷, C. Kobdaj¹¹⁸, M.K. Köhler¹⁰⁷, T. Kollegger¹¹⁰, A. Kondratyev⁷⁷, N. Kondratyeva⁹⁶, E. Kondratyuk⁹⁴, J. Konig⁷⁰, S.A. Konigstorfer¹⁰⁸, P.J. Konopka^{35,2}, G. Kornakov¹⁴⁴, S.D. Koryciak², L. Koska¹¹⁹, A. Kotliarov⁹⁸, O. Kovalenko⁸⁸, V. Kovalenko¹¹⁵, M. Kowalski¹²⁰, I. Králik⁶⁶, A. Kravčáková³⁹, L. Kreis¹¹⁰, M. Krivda^{113,66}, F. Krizek⁹⁸, K. Krizkova Gajdosova³⁸, M. Kroesen¹⁰⁷, M. Krüger⁷⁰, E. Kryshen¹⁰¹, M. Krzewicki⁴⁰, V. Kučera³⁵, C. Kuhn¹³⁹, P.G. Kuijer⁹³, T. Kumaoka¹³⁶, D. Kumar¹⁴³, L. Kumar¹⁰³, N. Kumar¹⁰³, S. Kundu^{35,89}, P. Kurashvili⁸⁸, A. Kurepin⁶⁵, A.B. Kurepin⁶⁵, A. Kuryakin¹¹¹, S. Kushpil⁹⁸, J. Kvapil¹¹³, M.J. Kweon⁶³, J.Y. Kwon⁶³, Y. Kwon¹⁴⁹, S.L. La Pointe⁴⁰, P. La Rocca²⁷, Y.S. Lai⁸², A. Lakrathok¹¹⁸, M. Lamanna³⁵, R. Langoy¹³², K. Lapidus³⁵, P. Larionov⁵³, E. Laudi³⁵, L. Lautner^{35,108}, R. Lavicka³⁸, T. Lazareva¹¹⁵, R. Lea^{142,24,59}, J. Lee¹³⁶, J. Lehrbach⁴⁰, R.C. Lemmon⁹⁷, I. León Monzón¹²², E.D. Lesser¹⁹, M. Lettrich^{35,108}, P. Lévai¹⁴⁷, X. Li¹¹, X.L. Li⁷, J. Lien¹³², R. Lietava¹¹³, B. Lim¹⁷, S.H. Lim¹⁷, V. Lindenstruth⁴⁰, A. Lindner⁴⁹, C. Lippmann¹¹⁰, A. Liu¹⁹, J. Liu¹³⁰, I.M. Lofnes²¹, V. Loginov⁹⁶, C. Loizides⁹⁹, P. Loncar³⁶, J.A. Lopez¹⁰⁷, X. Lopez¹³⁷, E. López Torres⁸, J.R. Luhder¹⁴⁶, M. Lunardon²⁸, G. Luparello⁶², Y.G. Ma⁴¹, A. Maevskaya⁶⁵, M. Mager³⁵, T. Mahmoud⁴⁴, A. Maire¹³⁹, M. Malaev¹⁰¹, Q.W. Malik²⁰, L. Malinina^{IV,77}, D. Mal'Kevich⁹⁵, N. Mallick⁵¹, P. Malzacher¹¹⁰, G. Mandaglio^{33,57}, V. Manko⁹¹, F. Manso¹³⁷, V. Manzari⁵⁴,

- Y. Mao⁷, J. Mareš⁶⁸, G.V. Margagliotti²⁴, A. Margotti⁵⁵, A. Marín¹¹⁰, C. Markert¹²¹,
 M. Marquard⁷⁰, N.A. Martin¹⁰⁷, P. Martinengo³⁵, J.L. Martinez¹²⁷, M.I. Martínez⁴⁶, G. Martínez
 García¹¹⁷, S. Masciocchi¹¹⁰, M. Masera²⁵, A. Masoni⁵⁶, L. Massacrier⁸⁰, A. Mastroserio^{141,54},
 A.M. Mathis¹⁰⁸, O. Matonoha⁸³, P.F.T. Matuoka¹²³, A. Matyja¹²⁰, C. Mayer¹²⁰,
 A.L. Mazuecos³⁵, F. Mazzaschi²⁵, M. Mazzilli³⁵, M.A. Mazzoni⁶⁰, J.E. Mdhluli¹³⁴,
 A.F. Mechler⁷⁰, F. Meddi²², Y. Melikyan⁶⁵, A. Menchaca-Rocha⁷³, E. Meninno^{116,30},
 A.S. Menon¹²⁷, M. Meres¹³, S. Mhlanga^{126,74}, Y. Miake¹³⁶, L. Micheletti^{61,25}, L.C. Migliorin¹³⁸,
 D.L. Mihaylov¹⁰⁸, K. Mikhaylov^{77,95}, A.N. Mishra¹⁴⁷, D. Miśkowiec¹¹⁰, A. Modak⁴,
 A.P. Mohanty⁶⁴, B. Mohanty⁸⁹, M. Mohisin Khan¹⁶, Z. Moravcova⁹², C. Mordasini¹⁰⁸,
 D.A. Moreira De Godoy¹⁴⁶, L.A.P. Moreno⁴⁶, I. Morozov⁶⁵, A. Morsch³⁵, T. Mrnjavac³⁵,
 V. Muccifora⁵³, E. Mudnic³⁶, D. Mühlheim¹⁴⁶, S. Muhuri¹⁴³, J.D. Mulligan⁸², A. Mulliri²³,
 M.G. Munhoz¹²³, R.H. Munzer⁷⁰, H. Murakami¹³⁵, S. Murray¹²⁶, L. Musa³⁵, J. Musinsky⁶⁶,
 C.J. Myers¹²⁷, J.W. Myrcha¹⁴⁴, B. Naik^{134,50}, R. Nair⁸⁸, B.K. Nandi⁵⁰, R. Nania⁵⁵, E. Nappi⁵⁴,
 M.U. Naru¹⁴, A.F. Nassirpour⁸³, A. Nath¹⁰⁷, C. Nattrass¹³³, A. Neagu²⁰, L. Nellen⁷¹,
 S.V. Nesbo³⁷, G. Neskovic⁴⁰, D. Nesterov¹¹⁵, B.S. Nielsen⁹², S. Nikolaev⁹¹, S. Nikulin⁹¹,
 V. Nikulin¹⁰¹, F. Noferini⁵⁵, S. Noh¹², P. Nomokonov⁷⁷, J. Norman¹³⁰, N. Novitzky¹³⁶,
 P. Nowakowski¹⁴⁴, A. Nyanin⁹¹, J. Nystrand²¹, M. Ogino⁸⁵, A. Ohlson⁸³, V.A. Okorokov⁹⁶,
 J. Oleniacz¹⁴⁴, A.C. Oliveira Da Silva¹³³, M.H. Oliver¹⁴⁸, A. Onnerstad¹²⁸, C. Oppedisano⁶¹,
 A. Ortiz Velasquez⁷¹, T. Osako⁴⁷, A. Oskarsson⁸³, J. Otwinowski¹²⁰, K. Oyama⁸⁵,
 Y. Pachmayer¹⁰⁷, S. Padhan⁵⁰, D. Pagano^{142,59}, G. Paić⁷¹, A. Palasciano⁵⁴, J. Pan¹⁴⁵,
 S. Panebianco¹⁴⁰, P. Pareek¹⁴³, J. Park⁶³, J.E. Parkkila¹²⁸, S.P. Pathak¹²⁷, R.N. Patra^{104,35},
 B. Paul²³, J. Pazzini^{142,59}, H. Pei⁷, T. Peitzmann⁶⁴, X. Peng⁷, L.G. Pereira⁷², H. Pereira Da
 Costa¹⁴⁰, D. Peresunko⁹¹, G.M. Perez⁸, S. Perrin¹⁴⁰, Y. Pestov⁵, V. Petráček³⁸, M. Petrovici⁴⁹,
 R.P. Pezzi^{117,72}, S. Piano⁶², M. Pikna¹³, P. Pillot¹¹⁷, O. Pinazza^{55,35}, L. Pinsky¹²⁷, C. Pinto²⁷,
 S. Pisano⁵³, M. Płoskoń⁸², M. Planinic¹⁰², F. Pliquette⁷⁰, M.G. Poghosyan⁹⁹, B. Polichtchouk⁹⁴,
 S. Politano³¹, N. Poljak¹⁰², A. Pop⁴⁹, S. Porteboeuf-Houssais¹³⁷, J. Porter⁸², V. Pozdniakov⁷⁷,
 S.K. Prasad⁴, R. Preghenella⁵⁵, F. Prino⁶¹, C.A. Pruneau¹⁴⁵, I. Pshenichnov⁶⁵, M. Puccio³⁵,
 S. Qiu⁹³, L. Quaglia²⁵, R.E. Quishpe¹²⁷, S. Ragoni¹¹³, A. Rakotozafindrabe¹⁴⁰, L. Ramello³²,
 F. Rami¹³⁹, S.A.R. Ramirez⁴⁶, A.G.T. Ramos³⁴, T.A. Rancien⁸¹, R. Raniwala¹⁰⁵, S. Raniwala¹⁰⁵,
 S.S. Räsänen⁴⁵, R. Rath⁵¹, I. Ravasenga⁹³, K.F. Read^{99,133}, A.R. Redelbach⁴⁰, K. Redlich^{V,88},
 A. Rehman²¹, P. Reichelt⁷⁰, F. Reidt³⁵, H.A. Reme-ness³⁷, R. Renfordt⁷⁰, Z. Rescakova³⁹,
 K. Reygers¹⁰⁷, A. Riabov¹⁰¹, V. Riabov¹⁰¹, T. Richert^{83,92}, M. Richter²⁰, W. Riegler³⁵,
 F. Riggi²⁷, C. Ristea⁶⁹, S.P. Rode⁵¹, M. Rodríguez Cahuantzi⁴⁶, K. Røed²⁰, R. Rogalev⁹⁴,
 E. Rogochaya⁷⁷, T.S. Rogoschinski⁷⁰, D. Rohr³⁵, D. Röhrich²¹, P.F. Rojas⁴⁶, P.S. Rokita¹⁴⁴,
 F. Ronchetti⁵³, A. Rosano^{33,57}, E.D. Rosas⁷¹, A. Rossi⁵⁸, A. Rotondi^{29,59}, A. Roy⁵¹, P. Roy¹¹²,
 S. Roy⁵⁰, N. Rubin²⁶, O.V. Rueda⁸³, R. Rui²⁴, B. Rumyantsev⁷⁷, P.G. Russek², A. Rustamov⁹⁰,
 E. Ryabinkin⁹¹, Y. Ryabov¹⁰¹, A. Rybicki¹²⁰, H. Rytkonen¹²⁸, W. Rzeszka¹⁴⁴, O.A.M. Saarimaki⁴⁵,
 R. Sadek¹¹⁷, S. Sadovsky⁹⁴, J. Saetre²¹, K. Šafářík³⁸, S.K. Saha¹⁴³, S. Saha⁸⁹, B. Sahoo⁵⁰,
 P. Sahoo⁵⁰, R. Sahoo⁵¹, S. Sahoo⁶⁷, D. Sahu⁵¹, P.K. Sahu⁶⁷, J. Saini¹⁴³, S. Sakai¹³⁶,
 S. Sambyal¹⁰⁴, V. Samsonov^{1,101,96}, D. Sarkar¹⁴⁵, N. Sarkar¹⁴³, P. Sarma⁴³, V.M. Sarti¹⁰⁸,
 M.H.P. Sas¹⁴⁸, J. Schambach^{99,121}, H.S. Scheid⁷⁰, C. Schiaua⁴⁹, R. Schicker¹⁰⁷, A. Schmah¹⁰⁷,
 C. Schmidt¹¹⁰, H.R. Schmidt¹⁰⁶, M.O. Schmidt¹⁰⁷, M. Schmidt¹⁰⁶, N.V. Schmidt^{99,70},
 A.R. Schmier¹³³, R. Schotter¹³⁹, J. Schukraft³⁵, Y. Schutz¹³⁹, K. Schwarz¹¹⁰, K. Schweda¹¹⁰,
 G. Scioli²⁶, E. Scomparin⁶¹, J.E. Seger¹⁵, Y. Sekiguchi¹³⁵, D. Sekihata¹³⁵, I. Selyuzhenkov^{110,96},
 S. Senyukov¹³⁹, J.J. Seo⁶³, D. Serebryakov⁶⁵, L. Šerkšnytė¹⁰⁸, A. Sevcenco⁶⁹, T.J. Shaba⁷⁴,
 A. Shabanov⁶⁵, A. Shabetai¹¹⁷, R. Shahoyan³⁵, W. Shaikh¹¹², A. Shangaraev⁹⁴, A. Sharma¹⁰³,
 H. Sharma¹²⁰, M. Sharma¹⁰⁴, N. Sharma¹⁰³, S. Sharma¹⁰⁴, O. Sheibani¹²⁷, K. Shigaki⁴⁷,
 M. Shimomura⁸⁶, S. Shirinkin⁹⁵, Q. Shou⁴¹, Y. Sibiriak⁹¹, S. Siddhanta⁵⁶, T. Siemarczuk⁸⁸,

T.F. Silva¹²³, D. Silvermyr⁸³, G. Simonetti³⁵, B. Singh¹⁰⁸, R. Singh⁸⁹, R. Singh¹⁰⁴, R. Singh⁵¹, V.K. Singh¹⁴³, V. Singhal¹⁴³, T. Sinha¹¹², B. Sitar¹³, M. Sitta³², T.B. Skaali²⁰, G. Skorodumovs¹⁰⁷, M. Slupecki⁴⁵, N. Smirnov¹⁴⁸, R.J.M. Snellings⁶⁴, C. Soncco¹¹⁴, J. Song¹²⁷, A. Songmoolnak¹¹⁸, F. Soramel²⁸, S. Sorensen¹³³, I. Sputowska¹²⁰, J. Stachel¹⁰⁷, I. Stan⁶⁹, P.J. Steffanic¹³³, S.F. Stiefelmaier¹⁰⁷, D. Stocco¹¹⁷, I. Storehaug²⁰, M.M. Storetvedt³⁷, C.P. Stylianidis⁹³, A.A.P. Suaiide¹²³, T. Sugitate⁴⁷, C. Suire⁸⁰, M. Suljic³⁵, R. Sultanov⁹⁵, M. Šumbera⁹⁸, V. Sumberia¹⁰⁴, S. Sumowidagdo⁵², S. Swain⁶⁷, A. Szabo¹³, I. Szarka¹³, U. Tabassam¹⁴, S.F. Taghavi¹⁰⁸, G. Taillepied¹³⁷, J. Takahashi¹²⁴, G.J. Tambave²¹, S. Tang^{137,7}, Z. Tang¹³¹, M. Tarhini¹¹⁷, M.G. Tarzila⁴⁹, A. Tauro³⁵, G. Tejeda Muñoz⁴⁶, A. Telesca³⁵, L. Terlizzi²⁵, C. Terrevoli¹²⁷, G. Tersimonov³, S. Thakur¹⁴³, D. Thomas¹²¹, R. Tieulent¹³⁸, A. Tikhonov⁶⁵, A.R. Timmins¹²⁷, M. Tkacik¹¹⁹, A. Toia⁷⁰, N. Topilskaya⁶⁵, M. Toppi⁵³, F. Torales-Acosta¹⁹, T. Tork⁸⁰, S.R. Torres³⁸, A. Trifiró^{33,57}, S. Tripathy^{55,71}, T. Tripathy⁵⁰, S. Trogolo^{35,28}, G. Trombetta³⁴, V. Trubnikov³, W.H. Trzaska¹²⁸, T.P. Trzcinski¹⁴⁴, B.A. Trzeciak³⁸, A. Tumkin¹¹¹, R. Turrisi⁵⁸, T.S. Tveter²⁰, K. Ullaland²¹, A. Uras¹³⁸, M. Urioni^{59,142}, G.L. Usai²³, M. Vala³⁹, N. Valle^{59,29}, S. Vallero⁶¹, N. van der Kolk⁶⁴, L.V.R. van Doremalen⁶⁴, M. van Leeuwen⁹³, P. Vande Vyvre³⁵, D. Varga¹⁴⁷, Z. Varga¹⁴⁷, M. Varga-Kofarago¹⁴⁷, A. Vargas⁴⁶, M. Vasileiou⁸⁷, A. Vasiliev⁹¹, O. Vázquez Doce¹⁰⁸, V. Vechernin¹¹⁵, E. Vercellin²⁵, S. Vergara Limón⁴⁶, L. Vermunt⁶⁴, R. Vértesi¹⁴⁷, M. Verweij⁶⁴, L. Vickovic³⁶, Z. Vilakazi¹³⁴, O. Villalobos Baillie¹¹³, G. Vino⁵⁴, A. Vinogradov⁹¹, T. Virgili³⁰, V. Vislavicius⁹², A. Vodopyanov⁷⁷, B. Volkel³⁵, M.A. Völk¹⁰⁷, K. Voloshin⁹⁵, S.A. Voloshin¹⁴⁵, G. Volpe³⁴, B. von Haller³⁵, I. Vorobyev¹⁰⁸, D. Voscek¹¹⁹, J. Vrláková³⁹, B. Wagner²¹, C. Wang⁴¹, D. Wang⁴¹, M. Weber¹¹⁶, R.J.G.V. Weelden⁹³, A. Wegrzynek³⁵, S.C. Wenzel³⁵, J.P. Wessels¹⁴⁶, J. Wiechula⁷⁰, J. Wikne²⁰, G. Wilk⁸⁸, J. Wilkinson¹¹⁰, G.A. Willems¹⁴⁶, E. Willsher¹¹³, B. Windelband¹⁰⁷, M. Winn¹⁴⁰, W.E. Witt¹³³, J.R. Wright¹²¹, W. Wu⁴¹, Y. Wu¹³¹, R. Xu⁷, S. Yalcin⁷⁹, Y. Yamaguchi⁴⁷, K. Yamakawa⁴⁷, S. Yang²¹, S. Yano^{47,140}, Z. Yin⁷, H. Yokoyama⁶⁴, I.-K. Yoo¹⁷, J.H. Yoon⁶³, S. Yuan²¹, A. Yuncu¹⁰⁷, V. Zaccole²⁴, A. Zaman¹⁴, C. Zampolli³⁵, H.J.C. Zanolí⁶⁴, N. Zardoshti³⁵, A. Zarochentsev¹¹⁵, P. Závada⁶⁸, N. Zaviyalov¹¹¹, H. Zbroszczyk¹⁴⁴, M. Zhalov¹⁰¹, S. Zhang⁴¹, X. Zhang⁷, Y. Zhang¹³¹, V. Zhrebchevskii¹¹⁵, Y. Zhi¹¹, D. Zhou⁷, Y. Zhou⁹², J. Zhu^{7,110}, Y. Zhu⁷, A. Zichichi²⁶, G. Zinovjev³ and N. Zurlo^{142,59}

^I Deceased^{II} Also at: Italian National Agency for New Technologies, Energy and Sustainable Economic Development (ENEA), Bologna, Italy^{III} Also at: Dipartimento DET del Politecnico di Torino, Turin, Italy^{IV} Also at: M.V. Lomonosov Moscow State University, D.V. Skobeltsyn Institute of Nuclear, Physics, Moscow, Russia^V Also at: Institute of Theoretical Physics, University of Wroclaw, Poland¹ A.I. Alikhanyan National Science Laboratory (Yerevan Physics Institute) Foundation, Yerevan, Armenia² AGH University of Science and Technology, Cracow, Poland³ Bogolyubov Institute for Theoretical Physics, National Academy of Sciences of Ukraine, Kiev, Ukraine⁴ Bose Institute, Department of Physics and Centre for Astroparticle Physics and Space Science (CAPSS), Kolkata, India⁵ Budker Institute for Nuclear Physics, Novosibirsk, Russia

- ⁶ California Polytechnic State University, San Luis Obispo, California, United States
- ⁷ Central China Normal University, Wuhan, China
- ⁸ Centro de Aplicaciones Tecnológicas y Desarrollo Nuclear (CEADEN), Havana, Cuba
- ⁹ Centro de Investigación y de Estudios Avanzados (CINVESTAV), Mexico City and Mérida, Mexico
- ¹⁰ Chicago State University, Chicago, Illinois, United States
- ¹¹ China Institute of Atomic Energy, Beijing, China
- ¹² Chungbuk National University, Cheongju, Republic of Korea
- ¹³ Comenius University Bratislava, Faculty of Mathematics, Physics and Informatics, Bratislava, Slovakia
- ¹⁴ COMSATS University Islamabad, Islamabad, Pakistan
- ¹⁵ Creighton University, Omaha, Nebraska, United States
- ¹⁶ Department of Physics, Aligarh Muslim University, Aligarh, India
- ¹⁷ Department of Physics, Pusan National University, Pusan, Republic of Korea
- ¹⁸ Department of Physics, Sejong University, Seoul, Republic of Korea
- ¹⁹ Department of Physics, University of California, Berkeley, California, United States
- ²⁰ Department of Physics, University of Oslo, Oslo, Norway
- ²¹ Department of Physics and Technology, University of Bergen, Bergen, Norway
- ²² Dipartimento di Fisica dell’Università ‘La Sapienza’ and Sezione INFN, Rome, Italy
- ²³ Dipartimento di Fisica dell’Università and Sezione INFN, Cagliari, Italy
- ²⁴ Dipartimento di Fisica dell’Università and Sezione INFN, Trieste, Italy
- ²⁵ Dipartimento di Fisica dell’Università and Sezione INFN, Turin, Italy
- ²⁶ Dipartimento di Fisica e Astronomia dell’Università and Sezione INFN, Bologna, Italy
- ²⁷ Dipartimento di Fisica e Astronomia dell’Università and Sezione INFN, Catania, Italy
- ²⁸ Dipartimento di Fisica e Astronomia dell’Università and Sezione INFN, Padova, Italy
- ²⁹ Dipartimento di Fisica e Nucleare e Teorica, Università di Pavia, Pavia, Italy
- ³⁰ Dipartimento di Fisica ‘E.R. Caianiello’ dell’Università and Gruppo Collegato INFN, Salerno, Italy
- ³¹ Dipartimento DISAT del Politecnico and Sezione INFN, Turin, Italy
- ³² Dipartimento di Scienze e Innovazione Tecnologica dell’Università del Piemonte Orientale and INFN Sezione di Torino, Alessandria, Italy
- ³³ Dipartimento di Scienze MIFT, Università di Messina, Messina, Italy
- ³⁴ Dipartimento Interateneo di Fisica ‘M. Merlin’ and Sezione INFN, Bari, Italy
- ³⁵ European Organization for Nuclear Research (CERN), Geneva, Switzerland
- ³⁶ Faculty of Electrical Engineering, Mechanical Engineering and Naval Architecture, University of Split, Split, Croatia
- ³⁷ Faculty of Engineering and Science, Western Norway University of Applied Sciences, Bergen, Norway
- ³⁸ Faculty of Nuclear Sciences and Physical Engineering, Czech Technical University in Prague, Prague, Czech Republic
- ³⁹ Faculty of Science, P.J. Šafárik University, Košice, Slovakia
- ⁴⁰ Frankfurt Institute for Advanced Studies, Johann Wolfgang Goethe-Universität Frankfurt, Frankfurt, Germany
- ⁴¹ Fudan University, Shanghai, China

- ⁴² Gangneung-Wonju National University, Gangneung, Republic of Korea
⁴³ Gauhati University, Department of Physics, Guwahati, India
⁴⁴ Helmholtz-Institut für Strahlen- und Kernphysik, Rheinische Friedrich-Wilhelms-Universität Bonn, Bonn, Germany
⁴⁵ Helsinki Institute of Physics (HIP), Helsinki, Finland
⁴⁶ High Energy Physics Group, Universidad Autónoma de Puebla, Puebla, Mexico
⁴⁷ Hiroshima University, Hiroshima, Japan
⁴⁸ Hochschule Worms, Zentrum für Technologietransfer und Telekommunikation (ZTT), Worms, Germany
⁴⁹ Horia Hulubei National Institute of Physics and Nuclear Engineering, Bucharest, Romania
⁵⁰ Indian Institute of Technology Bombay (IIT), Mumbai, India
⁵¹ Indian Institute of Technology Indore, Indore, India
⁵² Indonesian Institute of Sciences, Jakarta, Indonesia
⁵³ INFN, Laboratori Nazionali di Frascati, Frascati, Italy
⁵⁴ INFN, Sezione di Bari, Bari, Italy
⁵⁵ INFN, Sezione di Bologna, Bologna, Italy
⁵⁶ INFN, Sezione di Cagliari, Cagliari, Italy
⁵⁷ INFN, Sezione di Catania, Catania, Italy
⁵⁸ INFN, Sezione di Padova, Padova, Italy
⁵⁹ INFN, Sezione di Pavia, Pavia, Italy
⁶⁰ INFN, Sezione di Roma, Rome, Italy
⁶¹ INFN, Sezione di Torino, Turin, Italy
⁶² INFN, Sezione di Trieste, Trieste, Italy
⁶³ Inha University, Incheon, Republic of Korea
⁶⁴ Institute for Gravitational and Subatomic Physics (GRASP), Utrecht University/Nikhef, Utrecht, Netherlands
⁶⁵ Institute for Nuclear Research, Academy of Sciences, Moscow, Russia
⁶⁶ Institute of Experimental Physics, Slovak Academy of Sciences, Košice, Slovakia
⁶⁷ Institute of Physics, Homi Bhabha National Institute, Bhubaneswar, India
⁶⁸ Institute of Physics of the Czech Academy of Sciences, Prague, Czech Republic
⁶⁹ Institute of Space Science (ISS), Bucharest, Romania
⁷⁰ Institut für Kernphysik, Johann Wolfgang Goethe-Universität Frankfurt, Frankfurt, Germany
⁷¹ Instituto de Ciencias Nucleares, Universidad Nacional Autónoma de México, Mexico City, Mexico
⁷² Instituto de Física, Universidade Federal do Rio Grande do Sul (UFRGS), Porto Alegre, Brazil
⁷³ Instituto de Física, Universidad Nacional Autónoma de México, Mexico City, Mexico
⁷⁴ iThemba LABS, National Research Foundation, Somerset West, South Africa
⁷⁵ Jeonbuk National University, Jeonju, Republic of Korea
⁷⁶ Johann-Wolfgang-Goethe Universität Frankfurt Institut für Informatik, Fachbereich Informatik und Mathematik, Frankfurt, Germany
⁷⁷ Joint Institute for Nuclear Research (JINR), Dubna, Russia
⁷⁸ Korea Institute of Science and Technology Information, Daejeon, Republic of Korea

- ⁷⁹ *KTO Karatay University, Konya, Turkey*
- ⁸⁰ *Laboratoire de Physique des 2 Infinis, Irène Joliot-Curie, Orsay, France*
- ⁸¹ *Laboratoire de Physique Subatomique et de Cosmologie, Université Grenoble-Alpes, CNRS-IN2P3, Grenoble, France*
- ⁸² *Lawrence Berkeley National Laboratory, Berkeley, California, United States*
- ⁸³ *Lund University Department of Physics, Division of Particle Physics, Lund, Sweden*
- ⁸⁴ *Moscow Institute for Physics and Technology, Moscow, Russia*
- ⁸⁵ *Nagasaki Institute of Applied Science, Nagasaki, Japan*
- ⁸⁶ *Nara Women's University (NWU), Nara, Japan*
- ⁸⁷ *National and Kapodistrian University of Athens, School of Science, Department of Physics , Athens, Greece*
- ⁸⁸ *National Centre for Nuclear Research, Warsaw, Poland*
- ⁸⁹ *National Institute of Science Education and Research, Homi Bhabha National Institute, Jatni, India*
- ⁹⁰ *National Nuclear Research Center, Baku, Azerbaijan*
- ⁹¹ *National Research Centre Kurchatov Institute, Moscow, Russia*
- ⁹² *Niels Bohr Institute, University of Copenhagen, Copenhagen, Denmark*
- ⁹³ *Nikhef, National institute for subatomic physics, Amsterdam, Netherlands*
- ⁹⁴ *NRC Kurchatov Institute IHEP, Protvino, Russia*
- ⁹⁵ *NRC «Kurchatov»Institute - ITEP, Moscow, Russia*
- ⁹⁶ *NRNU Moscow Engineering Physics Institute, Moscow, Russia*
- ⁹⁷ *Nuclear Physics Group, STFC Daresbury Laboratory, Daresbury, United Kingdom*
- ⁹⁸ *Nuclear Physics Institute of the Czech Academy of Sciences, Řež u Prahy, Czech Republic*
- ⁹⁹ *Oak Ridge National Laboratory, Oak Ridge, Tennessee, United States*
- ¹⁰⁰ *Ohio State University, Columbus, Ohio, United States*
- ¹⁰¹ *Petersburg Nuclear Physics Institute, Gatchina, Russia*
- ¹⁰² *Physics department, Faculty of science, University of Zagreb, Zagreb, Croatia*
- ¹⁰³ *Physics Department, Panjab University, Chandigarh, India*
- ¹⁰⁴ *Physics Department, University of Jammu, Jammu, India*
- ¹⁰⁵ *Physics Department, University of Rajasthan, Jaipur, India*
- ¹⁰⁶ *Physikalisches Institut, Eberhard-Karls-Universität Tübingen, Tübingen, Germany*
- ¹⁰⁷ *Physikalisches Institut, Ruprecht-Karls-Universität Heidelberg, Heidelberg, Germany*
- ¹⁰⁸ *Physik Department, Technische Universität München, Munich, Germany*
- ¹⁰⁹ *Politecnico di Bari and Sezione INFN, Bari, Italy*
- ¹¹⁰ *Research Division and ExtreMe Matter Institute EMMI, GSI Helmholtzzentrum für Schwerionenforschung GmbH, Darmstadt, Germany*
- ¹¹¹ *Russian Federal Nuclear Center (VNIIEF), Sarov, Russia*
- ¹¹² *Saha Institute of Nuclear Physics, Homi Bhabha National Institute, Kolkata, India*
- ¹¹³ *School of Physics and Astronomy, University of Birmingham, Birmingham, United Kingdom*
- ¹¹⁴ *Sección Física, Departamento de Ciencias, Pontificia Universidad Católica del Perú, Lima, Peru*
- ¹¹⁵ *St. Petersburg State University, St. Petersburg, Russia*
- ¹¹⁶ *Stefan Meyer Institut für Subatomare Physik (SMI), Vienna, Austria*

- ¹¹⁷ *SUBATECH, IMT Atlantique, Université de Nantes, CNRS-IN2P3, Nantes, France*
- ¹¹⁸ *Suranaree University of Technology, Nakhon Ratchasima, Thailand*
- ¹¹⁹ *Technical University of Košice, Košice, Slovakia*
- ¹²⁰ *The Henryk Niewodniczanski Institute of Nuclear Physics, Polish Academy of Sciences, Cracow, Poland*
- ¹²¹ *The University of Texas at Austin, Austin, Texas, United States*
- ¹²² *Universidad Autónoma de Sinaloa, Culiacán, Mexico*
- ¹²³ *Universidade de São Paulo (USP), São Paulo, Brazil*
- ¹²⁴ *Universidade Estadual de Campinas (UNICAMP), Campinas, Brazil*
- ¹²⁵ *Universidade Federal do ABC, Santo Andre, Brazil*
- ¹²⁶ *University of Cape Town, Cape Town, South Africa*
- ¹²⁷ *University of Houston, Houston, Texas, United States*
- ¹²⁸ *University of Jyväskylä, Jyväskylä, Finland*
- ¹²⁹ *University of Kansas, Lawrence, Kansas, United States*
- ¹³⁰ *University of Liverpool, Liverpool, United Kingdom*
- ¹³¹ *University of Science and Technology of China, Hefei, China*
- ¹³² *University of South-Eastern Norway, Tønsberg, Norway*
- ¹³³ *University of Tennessee, Knoxville, Tennessee, United States*
- ¹³⁴ *University of the Witwatersrand, Johannesburg, South Africa*
- ¹³⁵ *University of Tokyo, Tokyo, Japan*
- ¹³⁶ *University of Tsukuba, Tsukuba, Japan*
- ¹³⁷ *Université Clermont Auvergne, CNRS/IN2P3, LPC, Clermont-Ferrand, France*
- ¹³⁸ *Université de Lyon, CNRS/IN2P3, Institut de Physique des 2 Infinis de Lyon , Lyon, France*
- ¹³⁹ *Université de Strasbourg, CNRS, IPHC UMR 7178, F-67000 Strasbourg, France, Strasbourg, France*
- ¹⁴⁰ *Université Paris-Saclay Centre d'Etudes de Saclay (CEA), IRFU, Département de Physique Nucléaire (DPhN), Saclay, France*
- ¹⁴¹ *Università degli Studi di Foggia, Foggia, Italy*
- ¹⁴² *Università di Brescia, Brescia, Italy*
- ¹⁴³ *Variable Energy Cyclotron Centre, Homi Bhabha National Institute, Kolkata, India*
- ¹⁴⁴ *Warsaw University of Technology, Warsaw, Poland*
- ¹⁴⁵ *Wayne State University, Detroit, Michigan, United States*
- ¹⁴⁶ *Westfälische Wilhelms-Universität Münster, Institut für Kernphysik, Münster, Germany*
- ¹⁴⁷ *Wigner Research Centre for Physics, Budapest, Hungary*
- ¹⁴⁸ *Yale University, New Haven, Connecticut, United States*
- ¹⁴⁹ *Yonsei University, Seoul, Republic of Korea*